acceptor pair spectra is resolvable even when one of the impurities produces a deep (here nearly 1 eV or ~ 0.4 E_g) bound state. It is likely that such structure may be observable in other semiconductors. If so, the ionization energies of deep centers may be accurately determined from the low-temperature pair luminescence spectrum alone.

ACKNOWLEDGMENTS

The authors are indebted to D. G. Thomas and F. A. Trumbore for advice and encouragement in the analysis of the pair transitions. Thanks are due to R. B. Zetterstrom and M. Kowalchik for providing many of the solution-grown crystals and to E. I. Gordon for the Ar^+ laser tube.

PHYSICAL REVIEW VOLUME 168, NUMBER 3 15 APRIL 1968

Quantum Theory of Transport in Narrow Channels

C. B. DUKE

General Electric Research and Development Center, Schenectady, New York 12301*
and
Department of Physics and Materials Research Laboratory, University of Illinois, Urbana, Illinois

(Received 1 December 1967)

The electrical conductivity in a semiconductor surface channel or a thin film is written in terms of integrals over a retarded current-current correlation function and evaluated using a Green's-function formulation of perturbation theory. The perturbation theory exhibits four new features. (1) The boundary conditions at the surfaces of the channel are expressed in terms of a fluctuation potential rather than a Fuchs reflectivity parameter. (2) The quantization of the eigenvalues for motion normal to the channel is explicitly incorporated into the theory. (3) The averaging procedure used to obtain the diagrammatic definition of the propagators and correlation functions is extended to include the effects both of screening and of graded interface impurity doping by permitting summation of multiple-scattering effects within planes of impurities parallel to the surface prior to the consideration of interference between these planes. (4) The propagators and conductivity are evaluated at arbitrary temperatures, using the Matsubara formalism. The conductivity is calculated explicitly in the quantum limit that the energy spacings ΔE between the eigenvalues for motion normal to the surface satisfy $\Delta E \gg kT$ for the occupied eigenstates. The approximations needed to reproduce the Boltzmann-equation analysis by Stern and Howard of the extreme quantum limit are delineated. The effects of dispersion and quantized-state mixing are examined for a δ-function model of the fluctuation potential. They are found to be significant if a quantized eigenvalue is near the Fermi energy or if the doping in the channel is highly nonuniform.

I. INTRODUCTION

THE theory of transport in thick films and semiconductor surface channels is an old and venerable topic, which is usually discussed within the framework of solving the Boltzmann equation, using classical or semiclassical carrier dynamics.[1–4] Although the possible importance of quantization effects in narrow channels or very thin films has been recognized for at least 10 years,[5] serious theoretical consideration of these effects has been given only in the past year.[6–10] The origin of this delay lies in the fact that although a variety of experiments have been interpreted as suggesting the importance of surface-induced quantization effects,[11–17] only recently have transport experiments[18] on (100) silicon surfaces convincingly demonstrated the existence of the two-dimensional energy bands associated with a narrow n-type inversion channel on p-type silicon.

The space-charge potential of an accumulation region at a planar n-type semiconductor interface is illustrated schematically in Fig. 1. Each quantized state for motion normal to the interface leads to a two-dimensional con-

* Permanent address.

[1] See, e.g., A. Many, Y. Goldstein, and N. B. Grover, *Semiconductor Surfaces* (North-Holland Publishing Co., Amsterdam, 1965), Chap. 4.
[2] R. F. Greene, Surface Sci. **2**, 101 (1964).
[3] R. F. Green, Phys. Rev. **141**, 687 (1966); **141**, 690 (1966).
[4] R. F. Greene and R. W. O'Donnell, Phys. Rev. **147**, 599 (1966).
[5] J. R. Schrieffer, in *Semiconductor Surface Physics*, edited by R. H. Kingston (University of Pennsylvania Press, Philadelphia, 1957), p. 68.
[6] C. B. Duke, Phys. Letters **24A**, 461 (1967).
[7] C. B. Duke, Phys. Rev. **159**, 632 (1967).
[8] D. J. BenDaniel and C. B. Duke, Phys. Rev. **160**, 679 (1967).
[9] F. Stern and W. E. Howard, Bull. Am. Phys. Soc. **12**, 275 (1967).
[10] F. Stern and W. E. Howard, Phys. Rev. **163**, 816 (1967).
[11] P. Handler and S. Eisenhouer, Surface Sci. **2**, 64 (1964).
[12] N. St. J. Murphy, Surface Sci. **2**, 86 (1964).
[13] F. Proix and P. Handler, Surface Sci. **5**, 81 (1966).
[14] F. F. Fang and W. E. Howard, Phys. Rev. Letters **16**, 797 (1966).
[15] A. P. VanGelder, Phys. Letters **22**, 7 (1966); T. W. Nee and R. E. Prange, *ibid.* **25A**, 582 (1967).
[16] S. Kawaji and Y. Kawaguchi, J. Phys. Soc. Japan Suppl. **21**, 336 (1966).
[17] S. Kawaji and H. C. Gatos, Surface Sci. **6**, 362 (1967); **7**, 215 (1967).
[18] A. B. Fowler, F. F. Fang, W. E. Howard, and P. J. Stiles, Phys. Rev. Letters **16**, 901 (1966); J. Phys. Soc. Japan Suppl. **21**, 331 (1966).

tinuum associated with motion parallel to the interface. In Fig. 1, we see the density of states $\rho_{11}(E+E_i)$ associated with the two-dimensional energy bands with minima which lie at the quantized-state eigenvalues $E=-E_i$. The density of states $\rho(E)$ associated with the three-dimensional continuum for $E>0$ is illustrated also.

For the potential and Fermi level shown in the figure, only the lowest quantized-state band is occupied at low temperatures T, i.e., as $kT\to 0$. The dynamics of the space-charge potential are governed by Poisson's equation and are discussed in Refs. 7, 9, and 10, and by BenDaniel and Duke[19] and Howard,[20] The quantum limit is defined to be that region of the space-charge parameters (high trapped charge and low temperature) in which the energy-level spacing between occupied and unoccupied states satisfies $\Delta E\gg kT$. Figure 1 constitutes an illustration of a special case of this limit. Stern and Howard[9,10] (SH) have given a Boltzmann-equation analysis of zero-temperature transport at Si and InAs surfaces in the extreme quantum limit that only the lowest two-dimensional band is occupied. They consider the scattering to be due to charged impurities either in the semiconductor or in the oxide of a field-effect junction. Such an analysis can give information only about the lowest quantized-state band, and it has been suggested that electromagnetic absorption[6,7] or tunneling[8] can give information on higher-lying bands also.

Our primary objective in this paper is the formulation of transport theory in narrow channels in such a way that the Fuchs boundary condition[2–4] does not enter the calculation. Such a formulation is necessary in the quantum limit because the concepts of specular and diffuse reflection become ill-defined. The Green's-function formalism[21,22] is ideally suited to this task because we calculate the "free" propagator in the average space-charge potential and treat the fluctuations of this potential, due either to impurities or irregularities in the surface, as a perturbation. Furthermore, the reduction of the Green's-function analysis to that of the Boltzmann equation is well known in three dimensions.[21,22] By a parallel reduction we are able to recover the starting equations used by SH[9,10] and thereby delineate the restrictions of, and corrections to, their results. We find, for example, that for space-charge channels in which either the impurity-density or impurity-potential form factor is nonuniform over the width of the channel, the corrections to the Boltzmann-equation analysis are considerably larger than in the case of a uniform system. Similarly, the possibility of moving the bottom of a localized-state band through the Fermi level (e.g., by increasing the gate voltage in a field-effect junction) causes dispersive effects and mobility reductions completely neglected in a Boltzmann-equation analysis. Therefore the Green's-function method provides a description of qualitatively new features of the transport process and is not merely a rederivation of the appropriate Boltzmann equation, as tends to be the case for uniform systems.[23]

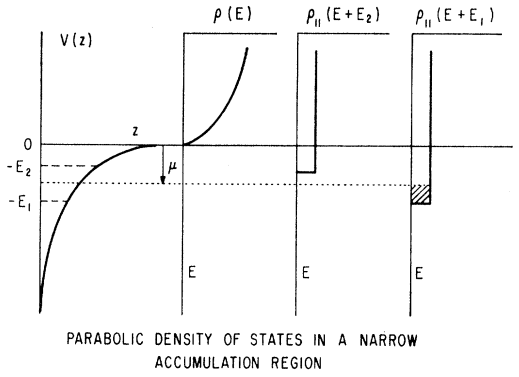

FIG. 1. Schematic illustration of the space-charge potential near the surface of a semi-infinite slab, $z>0$, of an n-type semiconductor. All energies are measured relative to the bottom of the conduction band in the bulk. The Fermi energy is denoted by μ. Each localized state in the discrete spectrum, $E<0$, is associated with a two-dimensional continuum due to motion parallel to the surface. The density of states $\rho_{11}(E)$ for these two-dimensional bands, as well as the three-dimensional density of states $\rho(E)$, is shown.

In keeping with our objective, the body of this paper is devoted to the comparatively "formal" topics of relating the surface conductivity to the current-current correlation function and evaluating the latter by use of Green's functions. Thus our work is complementary in outlook as well as scope to that of SH. Their main goal is the use of a simple, intuitive transport theory to calculate semiquantitatively the effect of screening, and hence gate voltage, on the charged-impurity-limited mobility of carriers in a narrow inversion layer. Ours, on the other hand, is the formulation and exploration of the features of the transport theory itself. To this end we utilize a simple δ-function ("contact-potential") model of the potential because it simplifies the calculations considerably. A reasonably complete analysis of the silicon data,[24] for example, requires both the careful consideration of the form of the potential given by SH, as well as the refinements of the transport theory discussed herein. A more extensive investigation of the consequences in InAs of the analytical results which we derive will be presented elsewhere.[25]

The definition of the model Hamiltonian and the derivation of the relation between the surface conductivity

[19] D. J. BenDaniel and C. B. Duke, Phys. Rev. **152**, 683 (1966).
[20] W. E. Howard (to be published).
[21] S. F. Edwards, Phil. Mag. **3**, 1020 (1958).
[22] A. A. Abrikosov, L. P. Gorkov, and I. E. Dzyaloshinski, *Methods of Quantum Field Theory in Statistical Physics* (Prentice-Hall, Inc., Englewood Cliffs, N. J., 1963), pp. 97–153, 315–317, 327–334.
[23] Only in the case of scattering from magnetic impurities has the Green's-function method led to qualitatively new results in three dimensions. See, e.g., A. A. Abrikosov, Physics **2**, 5, 61 (1965); S. D. Silverstein and C. B. Duke, Phys. Rev. Letters **18**, 695 (1967); Phys. Rev. **161**, 456 (1967); **161**, 470 (1967).
[24] F. F. Fang and A. B. Fowler (to be published).
[25] M. E. Alferieff and C. B. Duke, following paper, Phys. Rev. **168**, 832 (1968).

and the current-current correlation function are presented in Sec. II. Section III is devoted to the various topics associated with defining and evaluating the single-carrier propagator. These propagators are used to evaluate the correlation functions and conductivity in Sec. IV. All calculations are carried out for finite temperature, using the Matsubara formalism.[22,23] The impurity averages are carried out in Sec. III C in two different ways: in analogy to the procedure used in uniform systems,[21–23] and also in such a manner to incorporate all interference effects in planes of potential fluctuations parallel to the planar interface prior to the consideration of interference between the components of the carrier wave function scattered from the various planes. For convenience, an outline of the paper is given below.

II. SURFACE CONDUCTIVITY IN A NARROW CHANNEL

A. Linear Response in Inhomogeneous Systems

In this section, we review the coordinate-representation formulas describing the linear current response to an external electromagnetic field. In the following section, the general results are reduced to formulas for the nonlocal, frequency-dependent conductivity parallel to the surface in a narrow space-charge channel at a semiconductor (or semimetal) interface.

The linear current response to an external local vector potential $\mathbf{A}(\mathbf{x},t)$ is given by[22]

$$j_\nu(x)=-\frac{ne^2}{m_c c}A_\nu(x)+\frac{1}{c}\int dy^4\, P_{\nu\mu}{}^R(x,y)A_\mu(y)\,, \quad (2.1a)$$

$$P_{\nu\mu}{}^R(x,y)=\int_{-\infty}^{\infty}\frac{d\omega}{2\pi}e^{-i\omega(x_0-y_0)}P_{\nu\mu}{}^R(\mathbf{x},\mathbf{y},\omega)\,, \quad (2.1b)$$

in which the superscript R denotes retarded commutators, $x\equiv(\mathbf{x},x_0)$, $-e$ denotes the magnitude of the charge of a carrier (ultimately taken to be a Bloch electron), m_c denotes its effective mass, c is the speed of light, and n is the number of carriers per unit volume. The tensor polarization $P_{\mu\nu}{}^R$ is calculated, using the Matsubara formalism[22,23]:

$$P_{\mu\nu}{}^R(\mathbf{x},\mathbf{y},\omega)=P_{\mu\nu}(\mathbf{x},\mathbf{y},i\omega_n\to\omega+i\delta)\,, \quad (2.2a)$$

$$P_{\mu\nu}(\mathbf{x},\mathbf{y},i\omega_n)=\int_0^\beta d\tau\; e^{i\omega_n\tau}P_{\mu\nu}(\mathbf{x},\mathbf{y},\tau)\,, \quad (2.2b)$$

$$\omega_n=2\pi n/\beta\,, \quad (2.2c)$$

$$P_{\nu\mu}(\mathbf{x},\mathbf{y},\tau)=\langle T_\tau[j_{1\nu}(\mathbf{x},\tau)\,j_{1\mu}(\mathbf{y},0)]\rangle$$
$$=-(e^2\hbar^2/4m_c{}^2)\lim_{\mathbf{x}'\to\mathbf{x}}\lim_{\mathbf{y}'\to\mathbf{y}}(\nabla_{\mathbf{x}'}-\nabla_{\mathbf{x}})_\nu$$
$$\times(\nabla_{\mathbf{y}'}-\nabla_{\mathbf{y}})_\mu\langle T_\tau[\psi_\alpha(\mathbf{x},\tau)\psi_\beta(\mathbf{y},0)$$
$$\times\bar{\psi}_\beta(\mathbf{y}',0)\bar{\psi}_\alpha(\mathbf{x}',\tau)]\rangle\,, \quad (2.2d)$$

in which $\beta=(\kappa T)^{-1}$ is the reciprocal temperature, T_τ is the τ-ordering operator,[22] $\langle\ \rangle$ denotes thermal average over the grand-canonical ensemble, and $\psi(\mathbf{x},\tau)$ are the Matsubara field operators[22] for (Bloch) carriers.

In this paper, we consider only the scattering of carriers from random potential fluctuations due to impurities or inhomogeneities in the semiconductor interface. Electron-phonon[26] and electron-electron[27] interactions can be included in the formalism in the usual way. Using the effective-mass approximation[28] for the Bloch carriers, the Hamiltonian associated with a given spherical single-carrier ellipsoid is

$$H=H_0+H_I\,, \quad (2.3a)$$

$$H_0=\int d^3x\;\bar{\psi}_\alpha(\mathbf{x})\left[-\frac{\hbar^2\nabla^2}{2m_c}+V_e(\mathbf{x})\right]\psi_\alpha(\mathbf{x})\,, \quad (2.3b)$$

$$H_I=\int d^3x\;\bar{\psi}_\alpha(\mathbf{x})\Big[\sum_{\mathbf{R}_n}v_n(\mathbf{x}-\mathbf{R}_n)\Big]\psi_\alpha(\mathbf{x})\,. \quad (2.3c)$$

The use of the effective-mass approximation indicates that the $\psi_\alpha(\mathbf{x})$ are to be identified with the envelope functions of the Bloch carriers. The extension of the analysis to include more than one ellipsoid is straightforward.[7–10] The use of the n subscripts on the $v_n(\mathbf{x}-\mathbf{R}_n)$ denotes the fact that near a surface the form of the impurity potential depends explicitly on the distance of the impurity from the (planar) interface due to both screening effects and inhomogeneities in the interface. The external ("band-bending") potential is denoted by $V_e(\mathbf{x})$ and is the cause of the space-charge channels at semiconductor interfaces. The normal to the interface is taken in the z direction, so that a uniform magnetic field $\mathbf{H}$ oriented at an angle θ to the surface normal can

[26] See, e.g., G. D. Mahan and C. B. Duke, Phys. Rev. **149**, 705 (1966). More extensive references are given in this paper.
[27] J. S. Langer, Phys. Rev. **125**, 1003 (1961); O. Betheder-Matibet and P. Nozieres, Ann. Phys. (N. Y.) **37**, 17 (1966).
[28] W. Kohn, Solid State Phys. **5**, 258 (1957).

be inserted in (2.3b) by the substitutions[6,10]

$$\nabla \rightarrow \nabla - ie\mathbf{A}/\hbar c, \tag{2.4a}$$

$$\mathbf{A} = H(0, x\cos\theta - z\sin\theta, 0). \tag{2.4b}$$

The static electric field normal to the surface and static magnetic field are taken to determine the one-electron eigenfunctions in the absence of impurities via their inclusion in H_0. Schematically denoting these eigenfunctions by $\phi_s(x)$:

$$H_0\phi_s(\mathbf{x}) = E_s\phi_s(\mathbf{x}). \tag{2.5}$$

We define the noninteracting-particle representation for the field operators and single-particle propagators in the usual fashion[22]:

$$\psi(\mathbf{x},\tau) = \sum_s \phi_s(\mathbf{x})c_s(\tau), \tag{2.6a}$$

$$G(s',s,\tau) = -\langle T_\tau[c_{s'\alpha}(\tau)\bar{c}_{s\alpha}(0)]\rangle. \tag{2.6b}$$

A convenient form for the tensor polarization is the energy-representation expression

$$P_{v\mu}(\mathbf{x},\mathbf{y},i\omega_n) = -\frac{e^2\hbar^2}{4m_c^2}\sum_{s_1 s_4} W_v(s_1,s_4;\mathbf{x}) \times W_\mu(s_2,s_3,\mathbf{y})P(s_1,s_2,s_3,s_4;i\omega_n), \tag{2.7a}$$

$$W_v(s_i,s_j,\mathbf{x}) = [\phi_{s_i}(\mathbf{x})\nabla\bar{\phi}_{s_j}(\mathbf{x}) - \bar{\phi}_{s_j}(\mathbf{x})\nabla\phi_{s_i}(\mathbf{x})]_v, \tag{2.7b}$$

$$P(s_1,s_2,s_3,s_4;\tau) = \langle T_\tau[c_{s_1\alpha}(\tau)c_{s_2\beta}(0) \times \bar{c}_{s_3\beta}(0)\bar{c}_{s_4\alpha}(\tau)]\rangle. \tag{2.7c}$$

The longitudinal linear response is given in terms of diagrams by calculating directly the scalar polarization $P(i\omega_n)$ from the diagram shown in Fig. 2. In this case the many-body aspects of the calculation are incorporated entirely in the evaluation of $P(i\omega_n)$. A similar reduction of the consideration of many-body effects occurs also for transverse polarizations in the case of interband transitions near a symmetry point.[29] As noted in the Introduction, we shall primarily be concerned with calculating the static surface conductivity. Both in this case and in the analysis of the reflection and absorption of electromagnetic radiation at and near the surface, the distinction[30] between transverse and longitudinal response can be neglected because[31] if $\mathbf{q}$ is the wave vector and ω is the frequency of the electromagnetic field, then $\langle\mathbf{q}\cdot\mathbf{v}\rangle \sim \langle v\rangle\omega/c \ll \omega$ for electrons with average velocity $\langle v\rangle$. In this paper, we confine our attention to the calculation of the intraband contributions to the surface conductivity in the $\mathbf{q}\rightarrow 0$ limit.

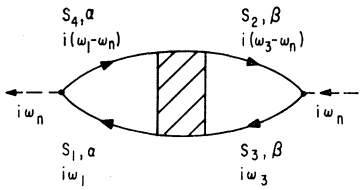

FIG. 2. Schematic diagram for the calculation of the scalar polarization function $P(s_1,s_2,s_3,s_4,i\omega_n)$. The irreducible vertex part is shown shaded.

B. Nonlocal, Frequency-Dependent Surface Conductivity

In this subsection, we give formulas for the conductivity when the perturbing electric field, to which the linear response is calculated, lies parallel to the semiconductor interface. This is the configuration for the usual static-surface-conductivity measurements[1,9–14,16–18] for both surface-barrier-electroreflectance[32–34] and some transverse-electroreflectance[35] experiments, and for measurements of surface effects on the microwave impedance.[15,36] It is not the configuration for Harrick's measurements of the surface absorption at infrared and higher frequencies.[7,37] Certain transitions between quantized-state bands are not excited unless the *a-c* field has a component normal to the surface.[7] Therefore an analysis of absorption and reflectivity measurements requires specification of the orientation of the polarization vector of the *ac* field relative to the surface.

The special case of Eqs. (2.7) relevant for the calculation of the static surface conductivity occurs when (a) the electric-field vector $\mathbf{E}$ lies parallel to the surface and (b) the spatial variation of the electric field normal to the surface is neglected over distances of the order of the thickness ($t\sim a_B$) of the space-charge channel. In the surface, the eigenfunctions of H_0 assume the form

$$\phi_s(\mathbf{x}) = \chi_\xi(z)\exp(i\mathbf{q}_{II}\cdot\boldsymbol{\varrho})/A, \tag{2.8a}$$

$$E_s = \tfrac{1}{2}\hbar^2\left(\frac{q_{II,1}^2}{m_c} + \frac{q_{II,2}^2}{m_c}\right) + \xi + \mu, \tag{2.8b}$$

in which μ is the chemical potential, A is the area of the planar interface, and $\boldsymbol{\varrho}$ is a vector in the (xy) plane of the interface. For convenience, we suppress the parallel subscript and use $\mathbf{q}$ to denote wave vectors parallel to the semiconductor interface. Equations (2.8) suggest the

[29] G. D. Mahan, Phys. Rev. **153**, 882 (1967).
[30] D. Pines and P. Nozieres, *Theory of Quantum Liquids, I* (W. A. Benjamin, Inc., New York, 1966), pp. 176–195, 251–260.
[31] See, e.g, J. M. Ziman, *Principles of the Theory of Solids* (Cambridge University Press, Cambridge, England, 1964), pp. 237–249.
[32] B. O. Seraphin and N. Bottka, Phys. Rev. **139**, A560 (1966); B. O. Seraphin, *ibid.* **140**, A1716 (1965); B. O. Seraphin and N. Bottka, *ibid.* **145**, 628 (1966).
[33] K. L. Shaklee, F. H. Pollak, and M. Cardona, Phys. Rev. Letters **15**, 883 (1965); M. Cardona, F. H. Pollak, and K. L. Shaklee, *ibid.* **16**, 644 (1966); Phys. Letters **23**, 37 (1966).
[34] J. Feinlieb, Phys. Rev. Letters **16**, 1200 (1966).
[35] V. Rehn and D. S. Keyser, Phys. Rev. Letters **18**, 848 (1967).
[36] J. F. Koch and C. C. Kuo, Phys. Rev. **143**, 470 (1966).
[37] N. J. Harrick, Phys. Rev. **125**, 1165 (1962).

Fourier decomposition of the vector potential

$$A_\mu(\mathbf{x},t)=A_\mu(\mathbf{q},z,\omega)e^{i\mathbf{q}\cdot\boldsymbol{\rho}}e^{-i\omega t}. \quad (2.9a)$$

Requirement (b) of homogeneity of $\mathbf{E}$ normal to the surface gives

$$A_\mu(\mathbf{q},z,\omega)\rightarrow A_\mu(\mathbf{q},\omega) \quad (2.9b)$$

for the vector potential. Taking the Fourier transform of Eq. (2.1a) with respect to $\boldsymbol{\rho}$ and t, we obtain

$$j_\nu(\mathbf{q},z,\omega)=-\frac{n(z)e^2}{m_c{}^2c}A_\nu(\mathbf{q},z,\omega)+\frac{1}{c}\int_{-\infty}^{\infty}dz' \times P^R{}_{\nu\mu}(\mathbf{q},z,z';\omega)A_\mu(\mathbf{q},z',\omega), \quad (2.10a)$$

$$P_{\nu\mu}(\mathbf{x},\mathbf{x}',i\omega_n)=\sum_{\mathbf{q}}\frac{e^{i\mathbf{q}\cdot(\boldsymbol{\rho}-\boldsymbol{\rho}')}}{A}P_{\nu\mu}(\mathbf{q},z,z';i\omega_n). \quad (2.10b)$$

The notation $n(z)$ is used for the carrier density in Eq. (2.10a). In narrow space-charge channels at temperature T, this density is given by[7,10,38]

$$n(z)=\frac{(2j+1)}{2\pi}\frac{m_c}{\hbar^2}\kappa T\sum_\xi F_0(-\xi/\kappa T)|\chi_\xi(z)|^2, \quad (2.11a)$$

$$F_0(x)=\ln[1+\exp(x)], \quad (2.11b)$$

in which j is the spin of the band associated with the mobile carriers. We have assumed that only the discrete spectrum in the narrow channel is occupied. A more general relation is given in Eqs. (2.6) and (2.7) of Ref. 38. The total surface current, which is the measured quantity in surface-transport experiments,[1] is obtained by integrating Eq. (2.10a) over z. For the case of an electric field independent of z in the surface channel we obtain

$$J_\nu(\mathbf{q},\omega)=[-(\Delta n_c e^2/m_c c)\delta_{\nu\mu}+P^R{}_{\nu\mu}(\mathbf{q},\omega)]A_\mu(\mathbf{q},\omega), \quad (2.12a)$$

$$\Delta n_c\equiv\int_{-\infty}^{\infty}n(z)dz, \quad (2.12b)$$

$$P^R{}_{\nu\mu}(\mathbf{q},\omega)=\int_{-\infty}^{\infty}dz\int_{-\infty}^{\infty}dz'\,P^R{}_{\nu\mu}(\mathbf{q},z,z',\omega). \quad (2.12c)$$

The surface conductivity is defined in terms of the total current to be

$$\Delta\sigma_{\nu\mu}(\mathbf{q},\omega)=-\omega^{-1}\,\mathrm{Im}P^R{}_{\nu\mu}(\mathbf{q},\omega), \quad (2.13)$$

in analogy with the definition of the bulk conductivity.[1,21,22] In writing Eqs. (2.12) and (2.13), we have ignored the bulk contribution to the current, so that $\Delta\sigma_{\nu\mu}$ is the change in conductance due to the presence of the surface channel, and Δn_c is the associated change in carrier concentration.[1]

Since nonlocal effects due to a nonzero photon wave vector $\mathbf{q}$ are small,[31] we neglect them by considering only $\mathbf{q}=0$ in Eqs. (2.9)–(2.13). The approximation of an electric field independent of z [Eq. (2.9b)] rules out consideration of an anomalous skin effect[31,39] due to carriers trapped in the space-charge region. However, in the case of localized charge at semiconductor interfaces, the maximum value[1,18] $\Delta n_c\sim10^{13}$ cm^{-2} implies that the surface charge leads to skin depths of the order of the thickness of the space-charge region only for frequencies in the optical region for which bulk interband absorption is usually the determining factor of the penetration depth. Therefore Eq. (2.9b) is a good approximation in the spectral regions of interest, and Eq. (2.13) is a direct measure of the surface impedance.[22,31]

III. EVALUATION OF THE SINGLE-PARTICLE PROPAGATOR

A. Free-Particle Propagator

The coordinate representation of the free-particle propagator is defined in terms of the eigenfunctions [Eq. (2.5)] of H_0. We consider only the case characterized by the absence of static magnetic fields normal to the surface, so that these eigenfunctions are given by Eq. (2.8). The coordinate representation of the free-particle propagator is given by

$$G_0(\mathbf{x}',\mathbf{x},i\omega_p)=\sum_{\mathbf{q},\xi}\frac{e^{i\mathbf{q}\cdot(\boldsymbol{\rho}'-\boldsymbol{\rho})}}{A}\frac{\chi_\xi(z')\bar{\chi}_\xi(z)}{i\omega_q-E(\mathbf{q})-\xi}, \quad (3.1a)$$

$$\omega_q=(2n+1)\pi/\beta, \quad (3.1b)$$

$$E(\mathbf{q})=\tfrac{1}{2}\hbar^2[q_1{}^2/m_c+q_2{}^2/m_c], \quad (3.1c)$$

$$[-(\hbar^2/2m_c)(d^2/dz^2)+V_e(z)-E]\chi_\xi(z)=0, \quad (3.1d)$$

$$E=\xi+\mu. \quad (3.1e)$$

The eigenvalue spectrum of Eq. (3.1d) is continuous for $E>0$ and discrete for $E<0$. A special case is illustrated in Fig. 1 for an accumulation region near the interface at $z=0$ of a semi-infinite semiconductor. In this paper, we confine our attention to calculating the low-temperature conductivity in the quantum limit that the occupation of the continuum states can be ignored and that $\Delta E_i=\Delta\xi\gg kT$. Using the quantum numbers $s=(\mathbf{q},\xi)$ to define the expansion (2.6a) of the field operator, and taking the carriers to be electrons, we find from (3.1a) that the energy representation of the free-electron propagator (2.6b) is given by

$$G_0(\mathbf{q}',\xi';\mathbf{q},\xi;i\omega_q)=\delta_{\mathbf{q}',\mathbf{q}}\delta_{\xi',\xi}G_0(\mathbf{q},\xi,i\omega_q), \quad (3.2a)$$

$$G_0(\mathbf{q},\xi,i\omega_q)=(i\omega_q-E(\mathbf{q})-\xi)^{-1}. \quad (3.2b)$$

We adopt the normalization

$$\int_{-\infty}^{\infty}\bar{\chi}_{\xi'}(z)\chi_\xi(z)dz=\delta_{\xi',\xi} \quad (3.3)$$

[38] Alan J. Bennett and C. B. Duke, Phys. Rev. **160**, 541 (1967).

[39] G. E. H. Reuter and E. H. Sondheimer, Proc. Roy. Soc. (London) **A195**, 336 (1948).

for the eigenfunctions of Eq. (3.1d) in the discrete spectrum. For convenience, Eq. (3.1d) for χ is solved subject to the model boundary condition

$$\chi_\xi(0)=0. \tag{3.4}$$

The exact boundary condition depends on the nature of the surface.[7] The solution of Eq. (3.1d) involves the specification of $V_e(z)$ as a self-consistent solution to Poisson's equation for the particular bulk sample and boundary conditions under consideration. A simple example of such a calculation is given in Ref. 7 for an accumulated surface. An evaluation of $V_e(z)$ for n-type inversion layers on p-type silicon has been given by Howard.[20]

The Fermi energy in each of the quantized-state bands ($E=-E_i$) is given by

$$E_{Fi}=E_i+\mu=-\xi. \tag{3.5}$$

Therefore at zero temperature a (discrete) band index $\xi>0$ corresponds to unoccupied bands and $\xi<0$ to occupied bands. The presence of impurities (or phonons, magnons) causes transitions both within and between the various two-dimensional quantized-state bands (for motion normal to the surface) associated with a local minimum in a given three-dimensional energy band.

B. Matrix Elements of the Fluctuation Potential

For convenience in writing the impurity potential and performing sums, we assume that the surface of the crystal is oriented so that the position $\mathbf{R}_n$ of an impurity can be decomposed uniquely according to

$$\mathbf{R}_n=\mathbf{R}_{\parallel}+\mathbf{R}_\perp, \tag{3.6a}$$

$$\mathbf{R}_{\parallel}\cdot\mathbf{n}=0, \tag{3.6b}$$

$$\mathbf{R}_\perp\cdot\boldsymbol{\rho}=0. \tag{3.6c}$$

Therefore $\mathbf{R}_{\parallel}$ is the coordinate of the impurity parallel to the surface (whose normal is denoted by $\mathbf{n}$), and $\mathbf{R}_\perp$ is its coordinate normal to that surface.

The conventional theories[21–23,27] of bulk impurity scattering consider impurity potentials of the form

$$V(\mathbf{x})=\sum_n v(\mathbf{x}-\mathbf{R}_n), \tag{3.7a}$$

$$v(\mathbf{x}-\mathbf{R}_n)=\sum_{\mathbf{k}} v(k)e^{i\mathbf{k}\cdot(\mathbf{x}-\mathbf{R}_n)}. \tag{3.7b}$$

All of the impurity atoms are characterized by the same spherically symmetric form factor $v(k)$. Equations (3.7) are inadequate to describe scattering from impurities near a surface for two reasons. First, the symmetry of the surface indicates a cylindrically symmetric rather than spherically symmetric form factor. Second, both the screening of charged impurities and the presence of additional potential fluctuations near the interface at $z=0$ cause the form factors themselves to be functions of $\mathbf{R}_\perp$. We simulate "surface scattering" by use of the dependence of the form factor (and, if necessary, the "impurity" density per unit area) on $\mathbf{R}_\perp$. Therefore we use the more general potential

$$V(\mathbf{x})=\sum_n v(\mathbf{R}_\perp;\ \mathbf{x}-\mathbf{R}_n), \tag{3.8a}$$

$$v(\mathbf{R}_\perp,\ \mathbf{x}-\mathbf{R}_n)=\sum_{\mathbf{q},k} v(R_\perp,\mathbf{q},k)e^{i\mathbf{q}\cdot(\rho-\mathbf{R}_{\parallel})}e^{ik(z-R_\perp)}. \tag{3.8b}$$

For a spherically symmetric potential,

$$v(\mathbf{R}_\perp,\mathbf{q},k)=v(\mathbf{R}_\perp,(q^2+k^2)^{1/2}). \tag{3.9}$$

The matrix elements of the impurity potential [Eqs. (3.8)] between the one-electron eigenstates (2.8) are

$$\langle\mathbf{q}_{j+1},\xi_{j+1}|\,V\,|\mathbf{q}_j,\xi_j\rangle = \sum_{\mathbf{R}_n} e^{i\Delta_j\cdot\mathbf{R}_{\parallel}}\langle\xi_{j+1}|\phi(\mathbf{R}_\perp,\boldsymbol{\Delta}_j)\,|\xi_j\rangle, \tag{3.10a}$$

$$\langle\xi_{j+1}|\phi(\mathbf{R}_\perp,\boldsymbol{\Delta}_j)\,|\xi_j\rangle \equiv\sum_k e^{-ikR_\perp}v(\mathbf{R}_\perp,\boldsymbol{\Delta}_j,k)M(k,\xi_{j+1},\xi_j), \tag{3.10b}$$

$$M(k,\xi_{j+1},\xi_j)=\int_{-\infty}^{\infty} e^{ikz}\bar{\chi}_{\xi_{j+1}}(z)\chi_{\xi_j}(z)dz), \tag{3.10c}$$

$$\boldsymbol{\Delta}_j\equiv\mathbf{q}_{j+1}-\mathbf{q}_j. \tag{3.10d}$$

The effective potential of an impurity at $\mathbf{R}_n=\mathbf{R}_\perp+\mathbf{R}_{\parallel}$ is the summand of Eq. (3.10a). The dependence of the form factor on $\mathbf{R}_\perp$ has the consequence that $\mathbf{R}_\perp$ no longer occurs solely in the phase factor $\exp(-ikR_\perp)$. Therefore averages over $\mathbf{R}_\perp$ no longer give conservation laws on k, as is the case for bulk impurity scattering. The off-diagonal components $\xi_{j+1}\neq\xi_j$ of $\langle\xi_{j+1}|\phi(\mathbf{R}_\perp,\boldsymbol{\Delta}_j)\,|\xi_j\rangle$ cause the mixing of eigenstates in different two-dimensional quantized-state bands by the impurity potential. In the case that more than one $\xi_j<0$, these transitions also can conserve energy, as shown in Fig. 3, and hence give important contributions to the resistivity.

C. Averages Over a Random Fluctuation Potential

In this subsection, we derive a diagrammatic prescription for constructing the one-electron propagator after averaging over a random distribution of impurity potentials. These results are well known for the bulk-impurity-scattering problem.[21–23,27] Therefore it is convenient to proceed by analogy, first summarizing the known consequences of the averaging for the bulk problem, and then introducing the new features of the surface analysis. Prior to the averaging process, the nth-order term for the one-electron propagator is given in both the bulk- and surface-scattering problems by

$$G^{(n)}(\mathbf{q}_n,\xi_n;\ \mathbf{q}_0,\xi_0;\ i\omega_q)=\sum_{\substack{q_1\cdots q_{n-1}\\ \xi_1\cdots\xi_{n-1}}}\prod_{i=0}^{n} G_0(\mathbf{q}_i,\xi_i;\ i\omega_q) \times\prod_{i=0}^{n-1}\langle\mathbf{q}_{i+1},\xi_{i+1}|\,V\,|\mathbf{q}_i,\xi_i\rangle. \tag{3.11}$$

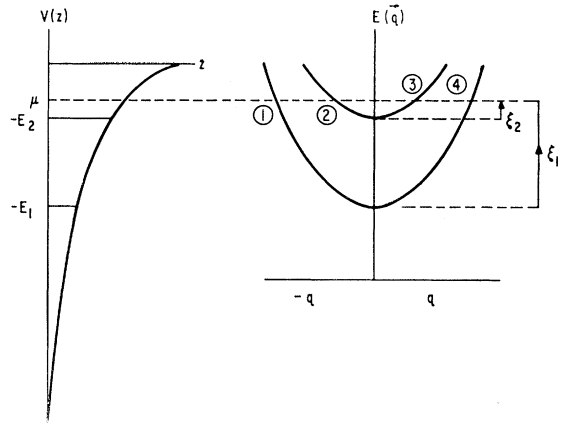

FIG. 3. Schematic illustration of the space-charge potential and the $E(\mathbf{q})$ eigenvalue spectrum for a case in which two quantized-state bands are occupied at zero temperature. Transitions rrom (1) to (4) and from (2) to (3) are energy-conserving intraband transitions at the Fermi surface, arising from the diagonal components of $\langle\xi_j|\phi(\mathbf{R}_\perp,\boldsymbol{\Delta}_j)|\xi_j\rangle$. Transitions from (1) to (2) and from (4) to (3) are energy-conserving interband transitions at the Fermi surface, arising from the off-diagonal components of $\langle\xi_{j+1}|\phi(\mathbf{R}_\perp,\boldsymbol{\Delta}_j)\times|\xi_j\rangle$ given by Eqs. (3.10) and (3.14) in the text.

In the case of bulk impurity scattering, the impurity potentials give rise in the nth-order diagram to the sum

$$S^{(n)}=\sum_{\{\mathbf{R}_j\}}\prod_{j=0}^{n-1}\exp[-i(\mathbf{q}_{j+1}-\mathbf{q}_j)\cdot\mathbf{R}_j]. \quad (3.12)$$

The diagonal terms in Eq. (3.12) (for which $\mathbf{R}_1=\mathbf{R}_2\cdots=\mathbf{R}_n$) give $c\delta_{\mathbf{q}_0,\mathbf{q}_n}$, with $c\equiv N_i/\Omega$, N_i being the number of impurity atoms and Ω the volume of the bulk crystal. The terms with only two $\mathbf{R}_j$ nonequal give terms $\mathcal{O}(c^2)$, and similarily for more complicated cluster terms. We recall that this procedure leads to the prescription[21,22] for an nth-order diagram of order c^m, $m\leq n$. For the electron propagator (after averaging):

(1) Draw dots representing the m-independent $\mathbf{R}_j$ values in Eq. (3.12).

(2) Connect these dots via n dashed interaction lines [associated with $v(\mathbf{q}_{i+1}-\mathbf{q}_i)$] to $(n+1)$-electron propagator lines [associated with $G_0(\mathbf{q}_i,i\omega_q)$] in all possible ways, subject to the conditions (a) of momentum conservation at each electron-interaction vertex and (b) that the total momentum transfer associated with the interaction lines emanating from a single dot be zero.

(3) Integrate over all $(n-m)$-independent internal $\mathbf{q}_i$ variables and multiply by c^m.

The concept of a proper self-energy is then introduced in the bulk calculation by observing that the contribution of each "irreducible" segment to the nth-order term in the propagator is independent of all the others. An irreducible segment is defined to be a subportion of a diagram which cannot be split into two disconnected parts by breaking a single propagator line. We use the independence of the contributions of these segments from each other to write the propagator as

$$G(\mathbf{q},i\omega_p)=\sum_{n=0}^{\infty}G^{(n)}(\mathbf{q},i\omega_p)$$
$$=G_0(\mathbf{q},i\omega_p)[1-G_0(\mathbf{q},i\omega_p)\Sigma(\mathbf{q},i\omega_p)]^{-1},$$

in which $\Sigma(\mathbf{q},i\omega_p)$ is the proper self-energy. This self-energy is calculated according to the rules (1)–(3), except that the two external propagator lines are removed from the nth-order diagram, and the subsidiary condition on rule (2) is added that one draws only those diagrams which cannot be divided into two topologically disconnected pieces by breaking a single-electron propagator line.

The evaluation of an nth-order diagram for the surface-transport propagator introduces two new features into the analysis: (a) The sum over $\mathbf{R}_{\perp,i}$ in the nth-order diagram is no longer just a sum over phase factors as in Eq. (3.12); and (b) the averaging does not require that the contribution associated with each irreducible segment be diagonal in the ξ_i variables, so that the proper self-energy must be defined by a matrix equation.

The sum in the general nth-order diagram [Eq. (3.11)] in the surface-transport case is given by

$$S^{(n)}=\sum_{\{\mathbf{R}_j\}}\prod_{j=0}^{n-1}\exp[-i\cdot(\mathbf{q}_{j+1}-\mathbf{q}_j)\cdot\mathbf{R}_{\parallel,j}]$$
$$\times\langle\xi_{j+1}|\phi(\mathbf{R}_{\perp j},\mathbf{q}_{j+1}-\mathbf{q}_j)|\xi_j\rangle. \quad (3.13)$$

It is convenient first to discuss the new feature (b) in the special case that the form factor $v(\mathbf{R}_\perp;\boldsymbol{\Delta}_j,k)$ is independent of $\mathbf{R}_\perp$, so that feature (a) does not occur. In this limit the matrix element in Eq. (3.13) becomes

$$\langle\xi_{j+1}|\phi(\mathbf{R}_\perp,\mathbf{q}_{j+1}-\mathbf{q}_j)|\xi_j\rangle$$
$$=\sum_{k_j}e^{-ik_jR_{\perp j}}\langle\xi_{j+1}|\phi(\mathbf{q}_{j+1}-\mathbf{q}_j,k_j)|\xi_j\rangle, \quad (3.14a)$$

$$\langle\xi_{j+1}|\phi(\mathbf{q}_{j+1}-\mathbf{q}_j,k_j)|\xi_j\rangle$$
$$=v(\mathbf{q}_{j+1}-\mathbf{q}_j,k_j)M(k_j,\xi_{j+1},\xi_j). \quad (3.14b)$$

Therefore we can perform the averaging prior to the k_j summations, with results essentially identical to the bulk results. The diagrammatic prescription for the nth-order contributions to the propagator proportional to c^m is:

(1) Draw dots representing the m-independent $\mathbf{R}_j$ values in Eq. (3.13).

(2) Connect these dots via n dashed interaction lines [associated with $\langle\xi_{j+1}|\phi(\mathbf{q}_{j+1}-\mathbf{q},k_j)|\xi_j\rangle$] to $n+1$ propagator lines [associated with $G_0(\mathbf{q}_j,\xi_j,i\omega_q)$] in all possible ways, subject to the conditions (a) of conservation of parallel momentum $\mathbf{q}$ at each propagator-interaction-line intersection and (b) that the total $\mathbf{q}$ and k transfer associated with the interaction lines emanating from a single dot be zero.

(3) Integrate over the $(n-m)$-independent $\mathbf{q}_j$, k_j variables and sum over the $(n-1)$-independent ξ_j variables.

The proper-self-energy matrix is given by

$$\mathbf{\Sigma}(\mathbf{q},i\omega_q)=\|\langle\xi'|\Sigma(\mathbf{q},i\omega_q)|\xi\rangle\|, \tag{3.15}$$

in which each matrix element $\langle\xi|\Sigma(\mathbf{q},i\omega_q)|\xi\rangle$ is defined to be the sum of all self-energy graphs associated with propagator graphs in which $G_0(\mathbf{q},\xi',i\omega_q)$ is the entering line, $G_0(\mathbf{q},i\omega_q)$ is the departing line, and the graph cannot be separated into two topologically disconnected parts by breaking an internal electron-propagator line. The propagator is given by

$$\mathbf{G}^{-1}(\mathbf{q},i\omega_q)=\mathbf{G}_0^{-1}(\mathbf{q},i\omega_q)-\mathbf{\Sigma}(\mathbf{q},i\omega_q), \tag{3.16a}$$

$$\mathbf{G}(\mathbf{q},i\omega_q)\equiv\|G(\mathbf{q},\xi',\xi,i\omega_q)\|, \tag{3.16b}$$

$$\mathbf{G}_0(\mathbf{q},i\omega_n)=\delta_{\xi',\xi}G_0(\mathbf{q},\xi,i\omega_q). \tag{3.16c}$$

Therefore the evaluation of the propagator involves both the evaluation of the matrix elements of the proper self-energy [Eq. (3.15)] and the inversion of the matrix (3.16a).

The second new feature in this surface-transport analysis, the dependence of the form factors on $\mathbf{R}_\perp$, arises both due to the screening of charge impurities and due to any spatial gradient, normal to the surface, of the density or character of the potential fluctuations. The change in character of the potential fluctuations, e.g., from fluctuations due to irregularities in the boundary layer to those due to impurity scattering, for different values of $\mathbf{R}_\perp$ suggests that the averages over $\mathbf{R}_{\perp,i}$ and $\mathbf{R}_{\|,i}$ of $S^{(n)}$ given by Eq. (3.13) should be performed separately. In the case of bulk scattering using the potential form factor given by Eqs. (3.7), the averaging is performed by a cluster expansion of $S^{(n)}$ in which, if $\mathbf{R}_{\|,i}=\mathbf{R}_{\|,j}$, then necessarily $\mathbf{R}_{\perp i}=\mathbf{R}_{\perp j}$. One might anticipate that a description of surface transport is more properly given by the two-step procedure of first averaging over $\mathbf{R}_\|$, in the same fashion in each plane of constant $\mathbf{R}_\perp$, and subsequently averaging over $\mathbf{R}_\perp$. The physical interpretation of this procedure for impurity scattering is that, by following it, we account for multiple-scattering interference effects separately for each plane of impurities parallel to the surface, and subsequently account for the interference between the various planes. For graded junctions and surfaces, only this modified prescription for the averaging is well defined. The average over $\mathbf{R}_\|$ generates a power-series expansion of the propagator in powers of $c_\|(\mathbf{R}_\perp)=N_{i,\|}(\mathbf{R}_\perp)/A$, where $N_{i,\|}(\mathbf{R}_\perp)$ is the number of impurities in a plane parallel to the surface at a distance $\mathbf{R}_\perp$ from it, and A is the area of this plane. For a uniform system, the $\mathbf{R}_\|$ average generates an expansion in $c_\|=c^{2/3}$, and the subsequent $R_\perp$ average multiplies this expansion by a second one in powers of $c_\perp=c^{1/3}$. Therefore the dual average generates a two-variable expansion of the proper self-energy in powers of $c_\|$ and $c_\perp$ which, for a uniform system, degenerates into the customary expansion in powers of c. The distinction between the bulk single average and surface dual average is irrelevant for a homogeneous fluctuation potential if one wants only the lowest-order linear term in c. However, for a graded junction the dual average is needed to calculate properly this term as a linear superposition of the terms in the dual average proportional to $c_\|(\mathbf{R}_\perp)$.

We next develop a modified diagrammatic perturbation theory for the calculation of the proper self-energy in the general case that (a) the potential form factors depend on $\mathbf{R}_\perp$ as indicated in Eqs. (3.8), and (b) the fluctuation potential is inhomogeneous in the direction normal to the surface, so that $c_\|(\mathbf{R}_\perp)=N_{i,\|}(\mathbf{R}_\perp)/A$ is explicitly a function of $\mathbf{R}_\perp$. It should be emphasized that in most practical numerical calculations[9,10] only that term which is the analog of the leading term in the expansion of the self-energy in powers of $c_\|$ and $c_\perp$ is considered. Although this term alone could be derived more simply then via the discussion given below, the fact that the formalism used by Stern and Howard[9,10] (SH) is implicitly but not manifestly equivalent to any of our averaging procedures suggests that a more thorough discussion of these procedures has utility. The discussion proceeds in three steps. First, we give a prescription for calculating the total self-energy after performing the $\mathbf{R}_\|$ average, but prior to performing the $\mathbf{R}_\perp$ average. Second, we consider the example of the uniform potential (3.14) and homogeneously doped sample to illustrate both the reduction to the conventional bulk-averaging procedure[21,22,27] and the definition of the proper self-energy after the $\mathbf{R}_\perp$ averaging has also been performed. Finally, we give the extension of this example to the case of graded doping and nonuniform potentials [Eq. (3.8)].

The prescription for generating (prior to averaging over $\mathbf{R}_\perp$) that nth-order term in the propagator which is proportional to

$$\prod_{i=1}^{m} c_\|(\mathbf{R}_{\perp i})$$

is:

(1) Draw $m<n$ dots associated with the m-independent values of $\mathbf{R}_\perp$ in the average of Eq. (3.13).

(2) Associate with each dot a value of $\mathbf{R}_{\perp i}$ $(i=1,\cdots,m)$ and connect the dots via n dashed interaction lines [associated with $\langle\xi_{j+1}|\phi(\mathbf{R}_{\perp i},\mathbf{q}_{j+1}-\mathbf{q}_j)|\xi_j\rangle$] to $n+1$ propagator lines [associated with $G_0(\mathbf{q}_j,\xi_j,i\omega_q)$] in all possible ways, subject to the conditions (a) of conservation of $\mathbf{q}$ at each propagator-interaction-line intersection and (b) that the total $\mathbf{q}$ transfer associated with each dot be zero.

(3) Integrate over the $(n-m)$-independent $\mathbf{q}_j$ variables, sum over the $(n-1)$-independent ξ_j variables, and multiply by

$$\prod_{i=1}^{m} c_\|(\mathbf{R}_{\perp i}).$$

The relation of this prescription for calculating propagator diagrams to the conventional bulk prescription[21,22,27] is illustrated by considering the equal-form-factor limit in which the interaction lines are associated with the potential (3.14), and $c_{\parallel}$ is independent of $\mathbf{R}_{\perp}$. To recover the fully averaged prescription given after Eqs. (3.14), we must perform the average over the $\mathbf{R}_{\perp}$ variables, with the assumption that $\mathbf{R}_{\perp i} \neq \mathbf{R}_{\perp j}$. Thus each dot is associated with a statistically independent impurity, and the $\mathbf{R}_{\perp}$ average gives the condition of $\sum_i k_i = 0$ for the k_i values associated with the interaction lines emanating from a single dot. The other limiting case, corresponding to accounting for interference effects within a plane of constant $\mathbf{R}_{\perp}$ prior to consideration of interference effects between the planes, consists of taking all of the $\mathbf{R}_{\perp i}$ values to be equal prior to averaging over $\mathbf{R}_{\perp}$. In general, we specify in a diagram those values of $\mathbf{R}_{\perp}$ which are taken to be equal in the final average by drawing a closed contour around the dots with equal $\mathbf{R}_{\perp i}$. The distinction between the bulk, coherent, and mixed selection of $\mathbf{R}_{\perp i}$ values is illustrated in Fig. 4.

The concept of a proper-self-energy diagram is defined only after all of the averages are complete. Thus Figs. 4(a) and 4(c) illustrate improper-self-energy diagrams, but Fig. 4(b) illustrates a proper-self-energy diagram because after the $\mathbf{R}_{\perp}$ average, all of the dots in the closed contours are associated with a single $\sum_i k_i = 0$ conservation rule. A general topological definition of a proper-self-energy diagram is one which cannot be split into two disconnected pieces by breaking a single propagator line. However, it is convenient to distinguish between *local* proper-self-energy diagrams, in which the enclosure of the impurity dots does not constitute a topological connection, and proper-self-energy diagrams, in which such an enclosure does constitute a topological connection. A variety of proper-self-energy diagrams is shown in Fig. 5.

For graded doping, it is desirable to use the above expansions of a local self-energy to formulate a perturbation theory, to which we refer as the coherent-parallel-plane (CPP) theory, in which interference effects within planes of fixed $\mathbf{R}_{\perp}$ are accounted for prior to consideration of interference between these planes. The essential ingredient of the CPP theory is our restatement of the averaging procedure in such a fashion that the averages over $\mathbf{R}_{\parallel}$ and $\mathbf{R}_{\perp}$ are separate. This added flexibility permits the summation of different subsets of self-energy diagrams than those usually considered in the bulk impurity case.[21,22,27] The appellation "coherent parallel plane" arises from the possibility of summing up all self-energy diagrams for motion in a given plane parallel to the interface prior to the evaluation of the total proper self-energy by performing the $\mathbf{R}_{\perp}$ averages. This particular subsummation proceeds in two steps. First, we construct the *local* proper-self-energy tensor to be the sum of the self-energy diagrams which (a) are associated with only one value of $\mathbf{R}_{\perp}$ and (b) are *local* proper-self-energy diagrams in the sense that interaction lines, but not enclosures of impurity dots, form topological connections between portions of the diagram. Such a construction is shown in Fig. 6. Terms proportional to $c_{\parallel}^{m}$,

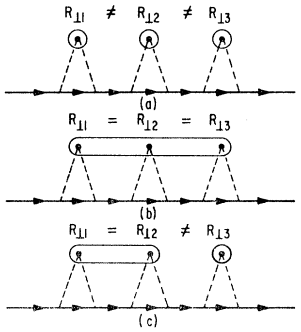

FIG. 4. Sixth-order perturbation-theory diagrams in which (a) illustrates the bulk-averaging procedure in which each independent value of $\mathbf{R}_{\parallel}$ is also associated with an independent value of $\mathbf{R}_{\perp}$, (b) illustrates the surface-coherence limit in which all of the independent $\mathbf{R}_{\parallel}$ values are associated with the same layer, and (c) illustrates a mixed case.

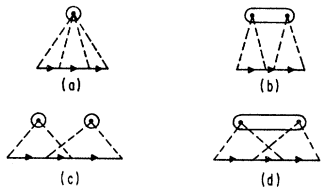

FIG. 5. Proper-self-energy diagrams in which the equal values of $\mathbf{R}_{\perp i}$ in the final $\mathbf{R}_{\perp}$ average are denoted by closed contours about the $\mathbf{R}_{\parallel}$ independent-impurity dots.

$m > 1$, arise from three sources: local proper-self-energy diagrams, like Fig. 5(d); local self-energy diagrams, like Fig. 5(b), in which only one $\mathbf{R}_{\perp}$ value is involved, but the diagram is not a local proper-self-energy diagram; and diagrams like Fig. 5(c), in which more than one value of $\mathbf{R}_{\perp}$ occurs. We wish to evaluate the subsum which consists of summing all contributions to the self-energy in which the $\mathbf{R}_{\perp}$ values are the same in higher-order terms in $c_{\parallel}(\mathbf{R}_{\perp})$. Thus the local-proper-self-energy tensor $\boldsymbol{\Sigma}(\mathbf{q},i\omega_q;\mathbf{R}_{\perp})$ is treated as a building block to be summed *prior* to the $\mathbf{R}_{\perp}$ average being performed. The coherent local proper-self-energy tensor $\boldsymbol{\Gamma}(\mathbf{q},i\omega_q;\mathbf{R}_{\perp})$ is defined to sum up the proper self-energy to all orders in $c_{\parallel}(\mathbf{R}_{\perp})$ for a given value of $\mathbf{R}_{\perp}$. It is given by

$$\boldsymbol{\Gamma}(\mathbf{q},i\omega_q;\mathbf{R}_{\perp}) = \boldsymbol{\Sigma}(\mathbf{q},i\omega_q,\mathbf{R}_{\perp})[1-\mathbf{G}_0(\mathbf{q},i\omega_q) \times \boldsymbol{\Sigma}(\mathbf{q},i\omega_q,\mathbf{R}_{\perp})]^{-1}, \quad (3.17a)$$

and is illustrated diagrammatically in Fig. 7, in which the wavy line denotes $\boldsymbol{\Gamma}(\mathbf{q},i\omega_q;\mathbf{R}_{\perp})$. We reemphasize that summing this selected subset of diagrams does not generate all the terms proportional to $c_{\parallel}^{m}$, $m > 1$, in the perturbation theory. For example, it omits Fig. 5(c), which is the usual[20] second-order term for homogeneous

systems. In fact, we define the coherent self-energy not so much because of its utility, but because it is the end result of systematically treating the system as an array of two-dimensional impurity planes (each with its own impurity density and potential form factors) from which the electron scatters independently. Therefore, summing the above subset of diagrams formalizes the intuitive approach of SH,[9,10] which utilizes only the "T-matrix" expansion for the self-energy illustrated in Fig. 8.

The total nth-order proper self-energy is obtained from the local self-energy by adding to rules (1)–(3) above the following final prescriptions:

(4) Draw only nth-order diagrams which are proper-self-energy diagrams (using both impurity-dot enclosures and interaction lines as topological connections).

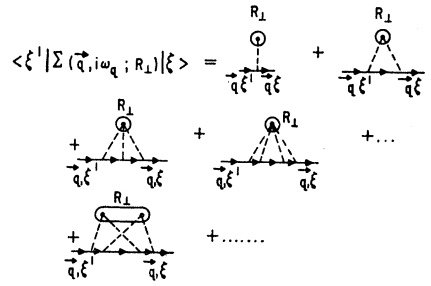

FIG. 6. Definition of the local proper self-energy $\langle\xi'|\Sigma(\mathbf{q},i\omega_q;\mathbf{R}_\perp)\times|\xi\rangle$ for motion in the plane parallel to the surface a distance $\mathbf{R}_\perp$ from the surface. For convenience, the external propagator lines have been retained in the diagrams, although they do not contribute to Σ. The fact that $\langle\xi'|\phi(\mathbf{R}_\perp,\mathbf{q}\to 0)|\xi\rangle$ does not vanish for a graded junction has been used in constructing the definition.

In a given diagram multiply by

$$\prod_{i=1}^{s} c_\perp(\mathbf{R}_{\perp i}),$$

corresponding to s-independent impurity-dot enclosures, and integrate over $d\mathbf{R}_{\perp i}$. This diagram then gives a contribution to the proper self-energy proportional to $c_{\parallel}{}^m c_\perp{}^s$.

(5) Sum over the possible topologically distinct nth-order diagrams.

The coherent proper-self-energy tensor

$$\boldsymbol{\Sigma}_c(\mathbf{q},i\omega_q)=\int dR_\perp\, c_\perp(R_\perp)\boldsymbol{\Gamma}(\mathbf{q},i\omega_q;R_\perp) \quad (3.17b)$$

corresponds to the sum of all self-energy diagrams linear in $c_\perp(\mathbf{R}_\perp)$, but of arbitrary order in $c_{\parallel}(\mathbf{R}_\perp)$, for a single value of $\mathbf{R}_\perp$. The conventional transport theory results from considering only those terms proportional to $c_{\parallel}(\mathbf{R}_\perp)$ which in turn, for a single-band model, are the T-matrix

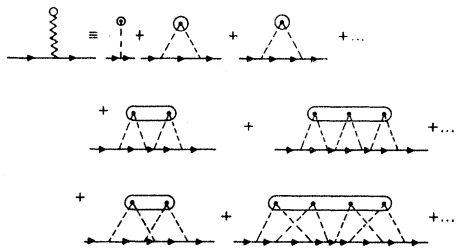

FIG. 7. Definition of the coherent self-energy of an electron due to the potential fluctuations in a plane parallel to the surface. It is not true that $\langle\xi'|\phi(\mathbf{R}_\perp,\mathbf{q})|\xi\rangle$ vanishes as $\mathbf{q}\to 0$ for a graded junction.

diagrams of Fig. 8 contributing to both $\boldsymbol{\Gamma}(\mathbf{q},i\omega_q;\mathbf{R}_\perp)$ and $\boldsymbol{\Sigma}(\mathbf{q},i\omega_q;\mathbf{R}_\perp)$.

D. Diagram Evaluation: Simple Example

In this subsection, we evaluate several low-order diagrams in the CPP theory and compare the results of this theory with those of Stern and Howard.[9,10] The underlying physical approximation in the SH model potential (Appendix B of Ref. 10) is that the space-charge channel is narrow relative to changes in the potential of a charged-impurity center. Interband-scattering matrix elements are expected to be small in such a limit because of the orthogonality of the $\chi_\xi(z)$. Therefore let us, for purposes of illustration of the interband-scattering effects, consider the opposite limit of a δ potential ("contact interaction") whose strength, however, can depend on its distance $R_\perp$ from the semiconductor surface. We use

$$v(R_\perp;\boldsymbol{\varrho}-\mathbf{R}_{\parallel},z-R_\perp)=v_\Omega(\mathbf{R}_\perp)\delta(\boldsymbol{\varrho}-\mathbf{R}_{\parallel})\delta(z-R_\perp), \quad (3.18a)$$

$$v(\mathbf{R}_\perp,\mathbf{q},k)=v_\Omega(\mathbf{R}_\perp), \quad (3.18b)$$

in which $v_\Omega(R_\perp)$ is the strength parameter with units of energy-volume. The use of Eq. (3.18) is well known to lead to certain pathological results.[40] However, this fact does not eliminate the utility of Eqs. (3.18) for our illustrative purposes.

The lowest-order contribution to the proper self-energy is that illustrated by the leading term in Figs.

FIG. 8. The "T-matrix" diagrams corresponding to the contributions to the proper self-energy which are linear in the total impurity concentration in the equal-form-factor case. The presence of the diagram with a single dashed line is a consequence of the fact that the first-order matrix element $\langle\xi'|\phi(\mathbf{R}_\perp,\mathbf{q})|\xi\rangle$ does not vanish as $\mathbf{q}\to 0$, and for graded junctions does not result in trivial subtractions.

[40] C. Herring, *Exchange Interactions Among Itinerant Electrons* (Academic Press Inc., New York, 1966), pp. 14, 15.

7 and 8:

$$\langle\xi_f|\Sigma^{(1)}(\mathbf{q}=0)|\xi_i\rangle=\int dR_\perp\, c(R_\perp) \times\langle\xi_f|\phi(R_\perp,\mathbf{q}=0)|\xi_i\rangle, \quad (3.19a)$$

$$c(R_\perp)\equiv c_{11}(R_\perp)c_\perp(R_\perp). \quad (3.19b)$$

It is convenient to perform the k sum in Eq. (3.14a) explicitly. Doing this, Eqs. (3.14) lead to

$$\langle\xi_f|\phi(R_\perp,\mathbf{q})|\xi_i\rangle=\int_{-\infty}^{\infty} dz\,\bar{\chi}_{\xi_f}(z)\chi_{\xi_i}(z) \times v(R_\perp,\mathbf{q},z-R_\perp), \quad (3.20)$$

which, for the δ potential, gives

$$\langle\xi_f|\phi(R_\perp,\mathbf{q})|\xi_i\rangle=\bar{\chi}_{\xi_f}(R_\perp)v_\Omega(R_\perp)\chi_{\xi_i}(R_\perp). \quad (3.21)$$

In the limit of equal form factors and homogeneous doping, the off-diagonal terms of (3.19a) are zero by the orthogonality of the χ_ξ, whereas the diagonal terms give the well-known[21,22,27,41–44] impurity-induced shifts of the bottom of the band of carriers, $\Delta E=v(\mathbf{q}=0,k=0)$. For graded junctions or spatially dependent form factors, the band shifts due to the diagonal terms in (3.19a) depend explicitly on ξ, and the off-diagonal terms no longer vanish. This result is a consequence of the spatial dependence of the average impurity potential. The matrix elements $\langle\xi'|\Sigma^{(1)}|\xi\rangle$ vanish if and only if the average impurity potential is incorporated into the definition of the external potential $V_e(\mathbf{x})$ in Eq. (2.3b).

In evaluating higher-order matrix elements of the proper self-energy, we consider the retarded self-energies obtained by the analytic continuation $i\omega_p\rightarrow\epsilon+i\delta$. The second-order contribution to Σ resulting from the second term in Figs. 7 and 8 is

$$\langle\xi_f|\Sigma^{(2)}(\mathbf{q},\epsilon)|\xi_i\rangle=\int dR_\perp\, c(R_\perp) \times\sum_{\xi'\mathbf{q}'}\langle\xi_f|\phi(R_\perp,\mathbf{q}-\mathbf{q}')|\xi'\rangle G(\xi',\mathbf{q}',\epsilon) \times\langle\xi'|\phi(R_\perp,\mathbf{q}'-\mathbf{q})|\xi_i\rangle. \quad (3.22)$$

If the free propagator G_0 is used in the intermediate state (as is customary in the one-band model), then the real part of the self-energy diverges logarithmically at gate voltages, for which a new ξ band moves through the Fermi energy. Thus the free-electron intermediate propagator is adequate for calculating the lifetime matrix

$$\langle\xi_f|\hbar/2\tau_0(\mathbf{q},\epsilon)|\xi_i\rangle\equiv i\,\mathrm{Im}\,\langle\xi_f|\Sigma^{(2)}(\mathbf{q},\epsilon)|\xi_i\rangle \equiv\langle\xi_f|\Gamma_0(\mathbf{q},\epsilon)|\xi_i\rangle, \quad (3.23)$$

but we must use a dressed propagator

$$G_\Gamma(\mathbf{q},\xi,\epsilon)=[\epsilon-E(\mathbf{q})-\xi+i\Gamma_0(\mathbf{q},\epsilon;\xi)]^{-1} \quad (3.24a)$$

to compute the real self-energy. We find for the δ potential at $T=0$

$$\Gamma_0(\mathbf{q},\epsilon,\xi)=\int dR_\perp\, c(R_\perp)|v_\Omega(R_\perp)|^2|\chi_\xi(R_\perp)|^2 \times\sum_{\xi'}|\chi_{\xi'}(R_\perp)|^2\pi\rho_{11}(\xi')\theta(\epsilon-\xi'), \quad (3.24b)$$

$$\langle\xi_f|\Sigma^{(2)}(\mathbf{q},\epsilon)|\xi_i\rangle=\int dR_\perp\, c(R_\perp)|v_\Omega(R_\perp)|^2\bar{\chi}_{\xi_f}(R_\perp)\chi_{\xi_i}(R_\perp) \times\sum_{\xi'}|\chi_{\xi'}(R_\perp)|^2F(E_0,\Gamma_0(\xi',\epsilon),\xi',\epsilon), \quad (3.25a)$$

$$F(E_0,\Gamma_0,\xi',\epsilon)=\rho_{11}(\xi')\left\{\frac{1}{2}\ln\left[\frac{\Gamma_0^2+(\xi'-\epsilon)^2}{\Gamma_0^2+E_0^2}\right] -i[\tan^{-1}(E_0/\Gamma_0)-\tan^{-1}((\xi'-\epsilon)/\Gamma_0)]\right\}, \quad (3.25b)$$

$$E[q_F(\xi)]=-\xi, \quad (3.26a)$$

$$\rho_{11}(\xi)=m(\xi)/2\pi\hbar^2, \quad (3.26b)$$

in which E_0 is a cutoff of the d^2q integrals due to our model potential not depending on $\mathbf{q}$, and $m(\xi)$ is the carrier mass in the ξ band (the values of m are not identical for all ξ in multivalley semiconductors). We again anticipate that for a uniform system the orthogonality of the χ_ξ will have the consequence of small off-diagonal matrix elements.

We next consider two additional types of diagrams which are not explicitly incorporated in the T-matrix approximation to the self-energy. These are the self-energy-insertion diagrams of the form illustrated in Fig. 9, and the crossing diagrams as illustrated in Fig. 10. The self-energy insertion illustrated in Fig. 9(b) has already been utilized implicitly by calculating Eq. (3.25) by use of (3.24). However, Eq. (3.24) takes into account only the lifetime effects associated with the self-energy insertion. Its use is conventional in bulk-resistivity calculations[21,22,27] for which the bottom of the impurity band lies far below the Fermi energy. However, from Eq. (3.25b) we see that as $|\xi|\rightarrow 0$ (i.e., the bottom of a quantized-state band moves through the Fermi energy), both dispersive as well as lifetime effects become impor-

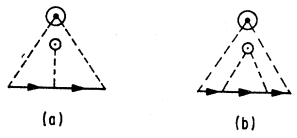

FIG. 9. The lowest-order self-energy insertions into the intermediate-state propagator of the second-order T-matrix diagram. These terms are proportional to $c(\mathbf{R}_{l1})c(\mathbf{R}_{l2})$ and therefore are of lower order in an expansion in powers of c.

[41] R. Parmenter, Phys. Rev. **97**, 587 (1955); **104**, 22 (1956).
[42] M. Lax and J. C. Phillips, Phys. Rev. **110**, 41 (1958).
[43] P. A. Wolff, Phys. Rev. **126**, 405 (1962).
[44] V. L. Bonch-Bruevich, Fiz. Tverd. Tela **4**, 2660 (1962) [English transl.: Soviet Phys.—Solid State **4**, 1953 (1963)].

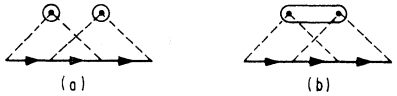

FIG. 10. The two lowest-order crossing diagrams omitted from the T-matrix approximation shown in Fig. 8.

tant. Thus, if we were to rigorously use perturbation theory in Eq. (3.25), we find that for a single quantized state the energy-shell dispersion relation is given by the solutions to

$$x=E(q)+E_D(\xi)\ln|x/E_0|\,, \tag{3.27a}$$

$$E_D(\xi)=\rho_{11}(\xi)\int dR_\perp\, c(R_\perp)|v_\Omega(R_\perp)|^2|\chi_\xi(R_\perp)|^4, \tag{3.27b}$$

$$x=\epsilon-\xi. \tag{3.27c}$$

The solution to Eqs. (3.27) indicates a shift to higher energies of the bottom of the ξ band. This shift occurs in addition to that given by Eqs. (3.19) and is a consequence of the strong ϵ dependence of the real self-energy as $|\xi|\to 0$. A proper treatment of these dispersive effects requires a solution to the Dyson equation illustrated in Fig. 11. The diagonal terms of this matrix equation are given by

$$\Sigma(\xi,\epsilon)-i\Gamma(\xi,\epsilon)=\sum_{\xi'} E_D(\xi,\xi')F(\xi',\epsilon)\,, \tag{3.28a}$$

$$E_D(\xi,\xi')=\rho_{11}(\xi')\int dR_\perp\, c(R_\perp)|v_\Omega(R_\perp)|^2 \times|\chi_\xi(R_\perp)|^2|\chi_{\xi'}(R_\perp)|^2, \tag{3.28b}$$

$$F(\xi,\epsilon)=\tfrac{1}{2}\ln\left|\frac{\Gamma^2(\xi,\epsilon)+[\xi-\epsilon+\Sigma(\xi,\epsilon)]^2}{\Gamma^2(\xi,\epsilon)+[E_0+\Sigma(\xi,\epsilon)]^2}\right| -i\left[\tan^{-1}\left(\frac{E_0+\Sigma(\xi,\epsilon)}{\Gamma(\xi,\epsilon)}\right) -\tan^{-1}\left(\frac{\xi-\epsilon+\Sigma(\xi,\epsilon)}{\Gamma(\xi,\epsilon)}\right)\right]. \tag{3.28c}$$

A more detailed discussion of the dispersive effects described by this equation will be given elsewhere.[25]

The contributions to the self-energy of the crossing diagrams illustrated in Fig. 10 may be written (for the δ potential) as

$$\langle\xi_f|\Sigma^{(i)}(\mathbf{q},i\omega_q)|\xi_i\rangle=\sum_{\xi_1\xi_2\xi_3} A^{(i)}(\xi_f,\xi_1,\xi_2,\xi_3,\xi_i) \times S(\xi_1,\xi_2,\xi_3,\mathbf{q},i\omega_q)\,, \tag{3.29a}$$

$$S(\xi_1,\xi_2,\xi_3,\mathbf{q},i\omega_q) =\sum_{\mathbf{q}_1,\mathbf{q}_2,\mathbf{q}_3}\prod_{s=1}^{3} G_\Gamma(\mathbf{q}_s,\xi_s,i\omega_q)\delta_{\mathbf{q}_3,\mathbf{q}_1+\mathbf{q}_2-\mathbf{q}}\,, \tag{3.29b}$$

$$A^{(a)}(\xi_f,\xi_1,\xi_2,\xi_3,\xi_i)=B(\xi_f,\xi_1,\xi_2,\xi_3)\bar{B}(\xi_1,\xi_2,\xi_3,\xi_i)\,, \tag{3.29c}$$

$$B(\xi_0,\xi_1,\xi_2,\xi_3)=\int dR_\perp\, c(R_\perp)|v_\Omega(R_\perp)|^2 \times\bar{\chi}_{\xi_0}(R_\perp)\chi_{\xi_1}(R_\perp)\bar{\chi}_{\xi_2}(R_\perp)\chi_{\xi_3}(R_\perp)\,, \tag{3.29d}$$

$$A^{(b)}(\xi_f,\xi_1,\xi_2,\xi_3,\xi_i)=\int dR_\perp\, c_{11}{}^2(R_\perp)c_\perp(R_\perp)|v_\Omega(R_\perp)|^4 \times\chi_{\xi_f}(R_\perp)\chi_{\xi_i}(R_\perp)\prod_{s=1}^{3}|\chi_{\xi_s}(R_\perp)|^2. \tag{3.29e}$$

The important aspect of these diagrams is that because of the δ function in Eq. (3.29b), for $\xi<0$ their order of magnitude is given by[22]

$$\mathrm{Im}\langle\xi|\Sigma^{(i)}|\xi\rangle\sim\Gamma_0(\Gamma_0/|\xi|), \quad |\xi|\gg\Gamma_0 \qquad \sim\Gamma_0, \quad \Gamma_0\lesssim|\xi|\,. \tag{3.30}$$

Therefore the crossing diagrams are of the same order of magnitude as the T-matrix diagrams when $|\xi|\sim\Gamma_0$.

We begin the comparison of our analysis with that of SH[9,10] by noting that in this subsection, we have utilized the δ potential [Eq. (3.18)] to illustrate the application of the prescriptions of the previous subsection to calculate some low-order diagrams. We find that in bands for which $|\xi|\lesssim\Gamma_0$, dispersive effects in real $\boldsymbol{\Sigma}(q,\epsilon)$ can substantially influence the self-energy and that crossing diagrams are not in general negligible relative to T-matrix diagrams. A numerical study of these effects, as well as those due to the off-diagonal matrix elements of the self-energy tensor, is given elsewhere.[25] The Born-approximation equations of SH[9,10] correspond to setting $\mathrm{Re}\,\langle\xi'|\Sigma(\mathbf{q},\epsilon)|\xi\rangle=0$ and using Eqs. (3.23) and (3.24b) to calculate the inverse lifetime τ^{-1}. The extra factor of $\cos\theta_{\mathbf{q}\cdot\mathbf{q}'}$ in their integrals arises from the vertex corrections (Sec. IV B) to the resistivity discussed in the next section of this paper. The SH phase-shift analysis corresponds to using the energy-shell T matrix in place of the potential matrix element in Eq. (3.24b). For the single-band model which they use, this result follows from a summation of the diagrams in Fig. 8 in a fashion exactly parallel to its well-known derivation in three dimensions.[21,22,27] Hence our evaluation of the self-energy dispersive effects and crossing diagrams constitute an estimate of the corrections to the Boltzmann-equation-type model used by SH. However, we reiterate that the emphasis is placed quite differently in our analysis than in that of SH. They are primarily concerned with

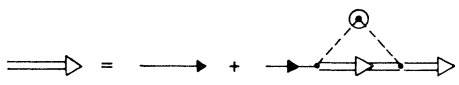

FIG. 11. The Dyson equation for the dressed propagator (denoted by the double solid line) in the second Born approximation. Only the diagonal components of the matrix equation are explicitly considered in the text.

a realistic evaluation of the potential and lowest-order scattering associated with charged impurities. We are primarily concerned with the structure of the transport theory itself and use the δ-model potential as a tool to illustrate various aspects of this structure. Therefore, as pointed out in the Introduction, the two analyses are complementary, and a thorough study of, e.g., the Si experiments,[24] must incorporate aspects of both.

IV. EVALUATION OF THE LOCAL SURFACE CONDUCTIVITY

A. Formal Specification of the Conductivity

In this subsection, we derive specific formulas for the surface conductivity $\Delta\sigma_{\mu\nu}$ given in Eq. (2.13) by using the surface-channel representation (2.8) in Eqs. (2.7) and (2.12c). Noting that for surface transport we want only $\mu,\nu=\{1,2\}$ in Eq. (2.13), the substitution of Eq. (2.8) into Eqs. (2.7) and (2.10b) leads to

$$P_{v\mu}(\mathbf{q},z,z',i\omega_n)=\frac{e^2\hbar^2}{m_c^2}\sum_{\xi_1\xi_2\xi_3\xi_4}\chi_{\xi_1}(z)\bar{\chi}_{\xi_4}(z)\chi_{\xi_2}(z')\bar{\chi}_{\xi_3}(z')$$
$$\times\sum_{\mathbf{p},i\omega_p}p_v\pi_\mu[\mathbf{p}_+;\,\xi_1,\xi_3,i\omega_p;\,\mathbf{p}_-,\xi_2,\xi_4,i(\omega_p-\omega_n)],\quad(4.1a)$$

$$\omega_n=2\pi n/\beta,\quad(4.1b)$$

$$\omega_p=(2n_p+1)\pi/\beta,\quad(4.1c)$$

$$\mathbf{p}_\pm=\mathbf{p}\pm\tfrac{1}{2}\mathbf{q}.\quad(4.1d)$$

The quantity π_μ is referred to as the vector-vertex function and is defined diagramatically in Fig. 12. The lowest-order contribution is given by

$$\pi_\mu^{(0)}[\mathbf{p}_+,\xi_1,\xi_3,i\omega_p;\,\mathbf{p}_-,\xi_2,\xi_4,i(\omega_p-\omega_n)]$$
$$=p_\mu\langle\xi_1|G(\mathbf{p}_+,i\omega_p)|\xi_3\rangle\langle\xi_2|G(\mathbf{p}_-,i(\omega_p-\omega_n)|\xi_4\rangle.\quad(4.2)$$

A simplification occurs when Eq. (4.1) is inserted into Eq. (2.13) for the conductivity, because the z' integration in Eq. (2.12c) gives a $\delta_{\xi_2\xi_3}$ factor in (4.1a), and the

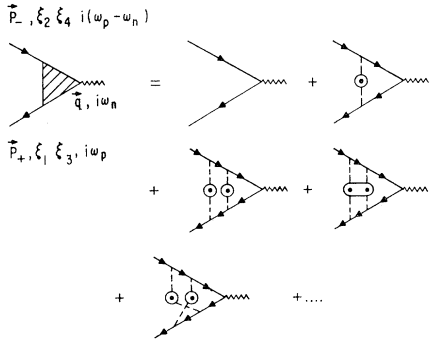

FIG. 12. Diagrammatic definition of the vector-vertex function $\pi_\mu(\mathbf{p}_+\xi_1,\xi_3,i\omega_p;\,\mathbf{p}_-\xi_4,\xi_2,i(\omega_p-\omega_n))$. The lowest-order vertex function is given by Eq. (4.2) in the text. Only those diagrams are included in the sum which contain no self-energy insertions on the propagator lines. The propagator lines are associated with the complete propagator matrices.

z integration gives a $\delta_{\xi_1\xi_4}$. Thus we regard

$$\sum_{\xi_2}\pi_\mu[\mathbf{p}_+,\xi_1,\xi_2,i\omega_p;\,\mathbf{p}_-,\xi_2,\xi_4,i(\omega_p-\omega_n)]$$
$$\equiv\langle\xi_1|\,\pi_\mu[\mathbf{p}_+,i\omega_p;\,\mathbf{p}_-,i(\omega_p-\omega_n)]\,|\xi_4\rangle\quad(4.3)$$

as the matrix elements of a matrix $\boldsymbol{\pi}_\mu$. Using this notation, Eq. (2.12c) becomes

$$P_{v\mu}(\mathbf{q},i\omega_n)=\frac{e^2\hbar^2}{m_c^2}\sum_{\mathbf{p}}p_vS_\mu(\mathbf{p}_+,\mathbf{p}_-,i\omega_n),\quad(4.4a)$$

$$S_\mu(\mathbf{p}_+,\mathbf{p}_-,i\omega_n)$$
$$=-\frac{1}{\beta}\sum_{\omega_p}\mathrm{Tr}\{\boldsymbol{\pi}_\mu[\mathbf{p}_+,i\omega_p;\,\mathbf{p}_-,i(\omega_p-\omega_n)]\},\quad(4.4b)$$

in which the Tr operator is defined with respect to the ξ index, and the sum over ω_p must be performed prior to the analytic continuation $i\omega_n\rightarrow\hbar\omega+i\delta$ needed to obtain $P^R{}_{v\mu}$ for use in Eq. (2.13). Equations (4.4), (4.3), and (2.13), together with Fig. 12, define the Green's-function calculation of the surface conductivity.

From Eq. (4.4) we see that the calculation of $\Delta\sigma$ consists of two steps: the evaluation of the vector-vertex matrix [Eq. (4.3)], and the performance of the $\mathbf{p}$ integral and ω_p sum in (4.4). The need for introducing the vector vertex arises because the contributions of all the first three terms on the right-hand side of the equation in Fig. 12 give contributions of equal order of magnitude to the vertex[21,22] in the limit that $|\Gamma_0|\ll|\xi|$. In analogy with the three-dimensional case,[21,22] the "ladder-diagram" contributions to the vector vertex are summed by solving the integral equation illustrated in Fig. 13 and given by

$$\boldsymbol{\pi}_\mu[\mathbf{p}_+,i\omega_p;\,\mathbf{p}_-,i(\omega_p-\omega_n)]=\mathbf{G}(\mathbf{p}_+,i\omega_p)$$
$$\times\Big\{p_\mu+\sum_{\mathbf{q}}\int dR_\perp\,c(R_\perp)\boldsymbol{\Phi}(R_\perp,\mathbf{q})\boldsymbol{\pi}_\mu$$
$$\times[\mathbf{p}_++\mathbf{q},\,i\omega_p;\,\mathbf{p}_-+\mathbf{q},\,i(\omega_p-\omega_n)]$$
$$\times\boldsymbol{\Phi}(R_\perp,-\mathbf{q})\Big\}\mathbf{G}(\mathbf{p}_-,i(\omega_p-\omega_n)),\quad(4.5a)$$

$$\boldsymbol{\Phi}(R_\perp,\mathbf{q})\equiv\|\langle\xi'|\phi(R_\perp,\mathbf{q})|\xi\rangle\|.\quad(4.5b)$$

The matrix elements $\langle\xi'|\boldsymbol{\phi}|\xi\rangle$ are given by Eqs. (3.10). When a band edge is near the Fermi surface, i.e., $|\xi|\rightarrow 0$, then in the component of $\boldsymbol{\pi}_\mu$ diagonal in ξ, other diagrams besides the ladder diagrams give contributions to Im $\pi\sim\Gamma_0$. This result is analogous to the

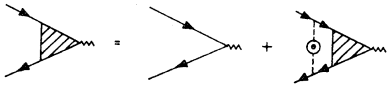

FIG. 13. Diagrammatic expression of the integral equation for the vector-vertex matrix which sums the ladder diagrams.

large contributions to the crossing diagrams in the self-energy and arises from the same cause: the failure of phase-space restrictions on intermediate-state propagators to give factors of $\Gamma_0/|\xi|\ll 1$. Thus we anticipate an enhanced resistivity in bands whose minima lie just below the Fermi energy.

The use of Eqs. (2.13), (3.22), (3.23), (3.24a), (4.4), and (4.5) gives the Green's-function approximation to the conductivity equivalent[21,22] to the Boltzmann-equation method of SH[9,10] but extended to the case of multiple occupied localized state bands. These equations, plus the diagrammatic prescription in Fig. 12 for calculating corrections to them, constitute the formal solution to the problem of calculating the conductivity for an arbitrary interaction and arbitrary quantized-state eigenvalue spectrum in the space-charge region.

B. Independent-Band Limit

In the case of an arbitrary impurity potential, the conductivity can be evaluated in closed form only in the independent-band limit in which the off-diagonal matrix elements of $\mathbf{\Phi}$ and $\mathbf{G}$ are taken to be zero in Eq. (4.5). We also require that for all occupied bands, $\Gamma_0(\xi)/|\xi|\ll 1$, so that the crossing diagrams are negligible. In this limit we replace G with G_Γ as given in Eqs. (3.23) and (3.24) and perform the analysis for an arbitrary interaction Φ. The use of the δ potential [Eq. (3.18)] leads to the vanishing of the "ladder-diagram" corrections illustrated in Fig. 13. Therefore the calculation of the conductivity is greatly simplified. However, the results of such a calculation remain sufficiently complicated and dependent on the details of the doping for graded interfaces that we defer discussion of them to another work.[25] It is evident that the independent-band limit will give us the two-dimensional analog of the three-dimensional Boltzmann-equation transport theory in each band. The technical aspects of our analysis differ from those of the well-known derivations[21,22] of this result in three dimensions only via our use of temperature-dependent retarded Green's functions rather than the zero-temperature time-ordered Green's functions. Therefore we present only an outline of the calculation.

Rather than solving Eq. (4.5a) for π_μ directly, it is customary to define $\mathbf{\Lambda}$ by

$$p_\mu \mathbf{\Lambda}(\mathbf{p},i\omega_p;\,\mathbf{q},i\omega_n)\equiv\sum_{\mathbf{q}}\int dR_\perp\, c(R_\perp)\mathbf{\Phi}(R_\perp,\mathbf{q})$$
$$\times\pi_\mu[\mathbf{p}_+ +\mathbf{q},\, i\omega_p;\, \mathbf{p}_- +\mathbf{q},\, i(\omega_p-\omega_n)]\mathbf{\Phi}(R_\perp,\mathbf{q}), \quad (4.6)$$

and solve for $\mathbf{\Lambda}$ via the use of

$$\mathbf{\Lambda}(\mathbf{p},i\omega_p;\,\mathbf{q},i\omega_n)=\int dR_\perp\, c(R_\perp)\sum_{\mathbf{p}'}\left(\frac{p'}{p}\right)$$
$$\times\cos\theta_{\mathbf{p}\cdot\mathbf{p}'}\mathbf{\Phi}(R_\perp,\,\mathbf{p}-\mathbf{p}')\mathbf{G}(\mathbf{p}_+',i\omega_p)\{1+\mathbf{\Lambda}(\mathbf{p}',i\omega_p,\mathbf{q},i\omega_n)\}$$
$$\times\mathbf{G}(\mathbf{p}_-',i(\omega_p-\omega_n))\mathbf{\Phi}(R_\perp,\,\mathbf{p}'-\mathbf{p}), \quad (4.7)$$

which is derived directly from Eq. (4.5a), assuming that $\mathbf{\Phi}(R_\perp,\,\mathbf{p}-\mathbf{p}')$ depends only on p, p', and $\cos\theta_{\mathbf{p}\cdot\mathbf{p}'}$.

In order to solve Eq. (4.7) for $\mathbf{\Lambda}$, we first note that only $S_\mu(\mathbf{p}_+,\mathbf{p}_-,i\omega_n)$ enters into Eq. (4.4). By first evaluating S_μ in terms of $\mathbf{\Lambda}$, we argue that the $\mathbf{p}'$ dependence of $\mathbf{\Lambda}$ can be ignored in the integral on the right-hand side of Eq. (4.7). From Eqs. (4.4), (4.5), and (4.6) we see that

$$S_\mu(\mathbf{p}_+,\mathbf{p}_-,i\omega_n)=\frac{1}{\beta}\sum_{\omega_p} p_\mu\,\mathrm{Tr}\{\mathbf{G}(\mathbf{p}_+,i\omega_p)$$
$$\times[1+\mathbf{\Lambda}(\mathbf{p},i\omega_p,\mathbf{q},i\omega_n)]\mathbf{G}[\mathbf{p}_-,\,i(\omega_p-\omega_n)]\}$$
$$=\frac{p_\mu}{2\pi i}\int_c dz f(z)\,\mathrm{Tr}\{\mathbf{G}(\mathbf{p}_+,z)$$
$$\times[1+\mathbf{\Lambda}(\mathbf{p},z;\,\mathbf{q},i\omega_n)]\mathbf{G}(\mathbf{p}_-,\,z-i\omega_n)\}, \quad (4.8a)$$
$$f(z)=[1+\exp(z/\kappa T)]^{-1}. \quad (4.8b)$$

The contour c and cuts of both the $\mathbf{G}$ and $\mathbf{\Lambda}$ factors are shown in Fig. 14. Performing the z integration first and then the analytic continuation $i\omega_n\rightarrow\hbar\omega+i\delta$ gives

$$S_\mu^R(\mathbf{p}_+,\mathbf{p}_-,\omega)=\frac{1}{\pi}\int_{-\infty}^{\infty} f(x)dx\; p_\mu\,\mathrm{Tr}[\mathbf{G}^R(\mathbf{p}_+,\,x+\hbar\omega)$$
$$\times\mathrm{Im}\{[1+\mathbf{\Lambda}^{RA}(\mathbf{p},x,\mathbf{q},\omega)]\mathbf{G}^A(\mathbf{p}_-,x)\}-\mathrm{Im}\{\mathbf{G}^R(\mathbf{p}_+,x)$$
$$\times[1+\mathbf{\Lambda}^{RA}(\mathbf{p},x,\mathbf{q},\omega)]\}G^A(\mathbf{p}_-,\,x-\hbar\omega)\}. \quad (4.9)$$

The surface conductivity is specified by Eqs. (2.12), (2.13), and (4.4) to be

$$\Delta\sigma_{v\mu}(\mathbf{q},\omega)=\frac{(2j+1)e^2\hbar^2}{m_c{}^2\omega}\sum_{\mathbf{p}} p_v\,\mathrm{Im}[S_\mu^R(\mathbf{p}_+,\mathbf{p}_-,\omega)], \quad (4.10)$$

where in writing all our results we use the conventions that $F^R\equiv\mathrm{Re}(F)-i\,\mathrm{Im}(F)$, and j is the spin of the carriers of effective mass m_c. For many-valley semiconductors an additional sum over valleys must be inserted into Eq. (4.10).

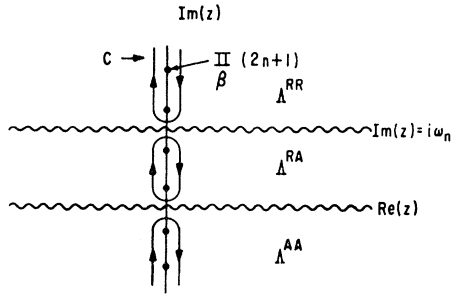

FIG. 14. The contour C for the evaluation of the integral in Eq. (4.8a) in the text. The cuts at $\mathrm{Im}z=0$ occur from both $\mathbf{G}(\mathbf{p}_+,z)$ and $\mathbf{\Lambda}(\mathbf{p},z;\,\mathbf{q},i\omega_n)$. The phases have been selected so that the cut in $\mathbf{\Lambda}$ lies infinitesimally below that of $\mathbf{G}$. The cuts at $\mathrm{Im}z=i\omega_n$ arise from a cut in $\mathbf{G}(\mathbf{p}_-,\,z-i\omega_n)$ placed infinitesimally above one in $\mathbf{\Lambda}(\mathbf{p},z,\mathbf{q},i\omega_n)$.

The important result to be noted in Eqs. (4.9) and (4.10) is that in calculations of the conductivity, the factor $\mathrm{Im}\langle\xi|G^R(\mathbf{p},x)|\xi\rangle\cong\pi\delta(x-E(\mathbf{p})-\xi)$ in Eq. (4.9) will project out a single value of $E(p)$ for a given x value. Furthermore, as $\omega\to 0$ for the uniform static conductivity, the two terms in Eq. (4.9) cancel unless $x\lesssim kT$. Therefore, in calculating the low-temperature conductivity, if $kT\ll|\xi|$ for the filled bands, then we must evaluate $\mathbf{\Lambda}(p,x,q=0,\omega\to 0)$ only on the Fermi surface of the various two-dimensional bands, i.e., at $|\mathbf{p}|=p_F(\xi)$ defined by Eq. (3.26a). This observation motivates the central approximation used in deriving the Boltzmann transport theory: the replacement $\mathbf{\Lambda}(\mathbf{p},i\omega_p,\mathbf{q},i\omega_n)\to\delta_{\xi'\xi}\langle\xi'|\Lambda(p_F(\xi),i\omega_p,\mathbf{q}=0,i\omega_n)|\xi\rangle$ in Eq. (4.7). In the independent-band limit this replacement reduces Eq. (4.7) to an algebraic equation for the diagonal matrix elements of $\mathbf{\Lambda}(p_F,i\omega_p,0,i\omega_n)$. The solution to the equation may be written as

$$\mathbf{\Lambda}=\mathbf{M}[1-\mathbf{M}]^{-1}, \tag{4.11a}$$

$$\langle\xi|M(\mathbf{p}_F(\xi),i\omega_p,i\omega_n)|\xi\rangle = \int dR_\perp\, c(R_\perp)\sum_{\mathbf{p}'}\cos\theta_{\mathbf{p}\cdot\mathbf{p}'}|\langle\xi|\phi(R_\perp,\mathbf{p}-\mathbf{p}')|\xi\rangle|^2 \times G_\Gamma[\mathbf{p}',\xi,i(\omega_p-\omega_n)]G_\Gamma(\mathbf{p}',\xi,i\omega_p), \tag{4.11b}$$

in which both $\mathbf{M}$ and $\mathbf{\Lambda}$ are diagonal matrices in the ξ index. The further approximation is made at this point that the $\mathbf{p}'$ dependence in ϕ is slow relative to that in the Green's functions. We obtain from Eq. (4.11b) the result

$$\langle\xi|M^{RA}(\mathbf{p},x,\omega)|\xi\rangle=\frac{1}{\tau_1(\mathbf{p},\xi)}\frac{i}{\omega-i/\tau_0(\mathbf{p},\xi)}, \tag{4.12a}$$

$$\frac{\hbar}{\tau_1(\mathbf{p},\xi)}=2\pi\rho_{11}(\xi)\int dR_\perp\, c(R_\perp)\int\frac{d\phi_{p'}}{2\pi} \times|\langle\xi|\phi(R_\perp,\mathbf{p}_F-\mathbf{p}_F')|\xi\rangle|^2\cos\theta_{\mathbf{p}\cdot\mathbf{p}'}, \tag{4.12b}$$

$$\frac{\hbar}{\tau_0(\mathbf{p},\xi)}=2i\,\mathrm{Im}\langle\xi|\mathbf{\Sigma}^{(2)}(\mathbf{p},0)|\xi\rangle=2\pi\rho_{11}(\xi)\int dR_\perp\, c(R_\perp) \times\int\frac{d\phi_{p'}}{2\pi}|\langle\xi|\phi(R_\perp,\mathbf{p}_F-\mathbf{p}_F')|\xi\rangle|^2. \tag{4.12c}$$

The final step in the evaluation of $\sigma_{\mu\nu}(0,\omega)$ is the insertion of Eqs. (4.11) and (4.12) into Eqs. (4.9) and (4.10). The $\mathbf{p}$ integral in Eq. (4.10) is performed first. To obtain the Boltzmann-equation result, we again use the approximation that τ_1 and τ_0 can be thought of as constants in the $\mathbf{p}$ integral because they vary slowly relative to the G_Γ factors which occur in Eq. (4.9) in the independent-band limit. Using this approximation and noting that the Tr operation in Eq. (4.9) reduces to a sum over filled-band indices $\xi<0$ in the independent-band limit, we obtain after some algebra

$$\sigma_{\nu\mu}(0,\omega)=\delta_{\nu\mu}\frac{(2j+1)e^2}{m_c{}^2}\sum_\xi\tfrac{1}{2}\rho_{11}(\xi)(\hbar^2p_F{}^2(\xi))\theta(-\xi) \times\int\frac{dx}{\hbar\omega}[f(x)-f(x+\hbar\omega)]\,\mathrm{Re}\left[\frac{i}{\omega+i/\tau(p_F,\xi)}\right], \tag{4.13a}$$

$$\hbar/\tau(p,\xi)=\hbar/\tau_0-\hbar/\tau_1 =2\pi\rho_{11}(\xi)\int c(R_\perp)dR_\perp\int\frac{d\phi_{p'}}{(2\pi)} \times|\langle\xi|\phi(R_\perp,\mathbf{p}_F-\mathbf{p}_F')|\xi\rangle|^2(1-\cos\theta_{\mathbf{p}\cdot\mathbf{p}'}). \tag{4.13b}$$

In the limit that $\omega\to 0$ we obtain the static conductivity

$$\sigma_{\nu\mu}(0,0)=\delta_{\nu\mu}\sum_\xi\frac{n(\xi)e^2\tau\theta(-\xi)}{m_c}, \tag{4.14a}$$

$$n(\xi)=(2j+1)p_F{}^2(\xi)/4\pi. \tag{4.14b}$$

Equations (4.13) and (4.14) are just the Born-approximation Boltzmann equations used by Stern and Howard,[9,10] as we anticipated from the analogy with the analysis in three dimensions.[21,22]

The above analysis can be generalized to include the case in which both the real and imaginary parts of the self-energy depend on ϵ but not on $\mathbf{p}$. The results, which are given in Ref. 25, are not quite equivalent to using $\tau(p_F,\xi)\to\tau(p_F,\xi,x)$ inside the integral in Eq. (4.13a). They reduce to this substitution only in the limits that $|x-\xi-\langle\xi|\mathrm{Re}\Sigma(x)|\xi\rangle|\gg\hbar/\tau(p_F,\xi,x)$ for all values of x which are important in the integral, and $\langle\xi|\mathrm{Re}\Sigma(x)|\xi\rangle$ can be regarded as constant over this range of values for x.

C. Synopsis and Discussion

In Sec. II, the surface conductivity due to carriers in a space-charge channel is formulated as the linear response to an electric field parallel to the channel. The evaluation of the conductivity in terms of a finite-temperature, retarded-propagator formalism is given in Sec. IV. In order to evaluate the propagators, a perturbation-theory, diagrammatic formalism is developed in Sec. III which utilizes averaging techniques suitable for the description of a random fluctuation potential. This potential is constructed to include the effects of scattering from the surface and of local variations in both the concentration and scattering potential of individual scattering centers. This extension of the bulk-conductivity calculation leads both to the necessity of incorporating the average fluctuation potential into the self-consistent definition of the one-electron channel potential and to modifications of the strength of various perturbation-theory diagrams. In the quantum limit the two-dimensional character of the localized-state energy bands causes both rapid changes in the single-particle

(and transport) lifetime with energy and logarithmic dispersion in the single-particle energy spectrum. Section IV B concludes the analysis with a specification of the approximations and limits needed to recover from the propagator theory the single-channel Boltzmann-equation analysis of Stern and Howard.[9,10]

As implied in the Introduction, the theory in this paper is developed primarily for its application to the description of surface transport in narrow channels at the semiconductor surface in a field-effect device.[1,5,9–14,16–18] Its application to the analysis of transport at InAs surfaces is given elsewhere.[25] An important aspect of transport in semiconductor surface channels is the tendency of these channels to form "one-dimensional atoms" at low temperatures when they trap enough charge to form a degenerate Fermi gas. The appellation "atom" is used because the width of these regions is $t\sim a_B$, and the energy spacing of the localized-state eigenvalues (for motion normal to the surface) is $\sim$1–10 times the shallow-donor (acceptor) binding energy. In such channels the quantum limits of $\Delta E_{ij}>[\kappa T,\Gamma_0(\xi_i),\Gamma_0(\xi_j)]$ can be achieved for good surfaces at helium temperatures. As the temperature or surface roughness is increased until $\Delta E_{ij}\sim[\kappa T,\Gamma_0(\xi_i),\Gamma_0(\xi_j)]$, the quantum theory developed herein goes over into the well-known semiclassical Boltzmann-equation theory[1–5,45] for transport in systems which are macroscopically inhomogeneous, but, unlike our case, are microscopically homogeneous. A quantum theory is required in the limit of the channel width becoming sufficiently small that the microscopic-homogeneity condition is violated. This situation also can exist in other systems, like continuous very thin films.[46,47]

Previous theoretical analyses[46] of quantum size effects in thin bismuth films have neglected both the inhomogeneity of the potential form factors and the dispersive effects discussed in Sec. III D. In fact, we show in Ref. 25 that the neglect of the dispersive effects substantially alters the calculated results for both equilibrium and transport properties. Therefore the calculation of the properties of thin bismuth films should be reexamined using our more general perturbation theory.

Finally, it is evident that in the quantum limit our transport theory is similar to that of a dilute, random alloy,[23,41,48–52] but in two rather than three dimensions. Therefore many features of transport in these alloys have analogs in the quantum theory of transport in narrow channels. An example of current interest is the Kondo effect,[23] which occurs when the scattering centers exhibit the spin-dependent potential $V(\mathbf{x}-\mathbf{R}_s)=\boldsymbol{\sigma}\cdot\mathbf{S}_s J\times(\mathbf{x}-\mathbf{R}_s)$. The perturbation theory developed by Abrikosov[23] can be trivially extended to the narrow-channel situation via replacing multiplication by the concentraction c with multiplication by $c(\mathbf{R}_\perp)$ and integration over $R_\perp$, using at each fermion-pseudofermion intersection the interaction $\langle\xi'|J(\mathbf{R}_\perp,q)|\xi\rangle$ defined using Eqs. (3.14). All sums over ξ' variables are performed in accord with the prescriptions in Sec. III C. The logarithmic divergence of $\langle\xi|\mathrm{Im}\Sigma^{(3)}(\mathbf{q},\epsilon)|\xi\rangle$ as $\epsilon\to 0$ occurs in our theory in exact analogy with its occurrence in the theory of three-dimensional dilute magnetic alloys. The new analytical feature of the Kondo effect in two dimensions is the exact rather than approximate constancy of the density of states inside the perturbation-theory integrals. The new physical feature of the surface-channel system, important for both the Kondo effect and other many-body effects, is the possibility of varying the density of the degenerate-electron fluid by varying the gate voltage. Therefore the properties (and in particular the phase diagram) of the fluid can be studied experimentally, using a given sample in which both the temperature and density of the fluid can be controlled both reversibly and in a relatively simple fashion. This fact renders the surface-channel system as an outstanding possible test case for the various many-body theories of the electron gas and, in particular, for theories of its collective magnetic and superconducting behavior.

ACKNOWLEDGMENTS

The author is greatly indebted to Dr. F. Stern and Dr. W. E. Howard for several stimulating discussions and for a copy of their work prior to publication.

[45] A recent review of the semiclassical transport theories of surface conductivity has been given by D. R. Frankl, *Electrical Properties of Semiconductor Surfaces* (Pergamon Press, Inc., New York, 1967), Chap. 4.

[46] B. A. Tavger and V. Ya. Demikhovskii, Fiz. Tverd. Tela **5**, 644 (1963) [English transl.: Soviet Phys.—Solid State **5**, 469 (1963)]; V. B. Sandomirskii, Zh. Eksperim. i Teor. Fiz. **52**, 158 (1967) [English transl.: Soviet Phys.—JETP **25**, 101 (1967)]; I. O. Kulik, JETP Pis'ma v Redaktsiyu **5**, 423 (1967) [English transl.: Soviet Phys.—JETP Letters **5**, 345 (1967)].

[47] Yu. F. Ogrin, V. N. Lutskii, and M. I. Elinson, JETP Pis'ma v Redaktsiyu **3**, 114 (1966) [English transl.: Soviet Phys.—JETP Letters **3**, 71 (1966)].

[48] S. F. Edwards, Proc. Roy. Soc. (London) **A267**, 518 (1962).

[49] J. L. Beeby, Proc. Roy. Soc. (London) **A279**, 82 (1964).

[50] A. W. B. Taylor, Physica **32**, 2030 (1966).

[51] P. Lloyd, Proc. Phys. Soc. (London) **90**, 207 (1967).

[52] E. J. Moore, Phys. Rev. **160**, 607 (1967); **160**, 618 (1967).